AFAPL-TR-70-21

HYDROGEN FLUORIDE TRACER MOLECULE SPECTROSCOPY APPLIED TO TURBULENT MIXING AND COMBUSTION

P. C. Malte

J. A. Nicholls

The University of Michigan

TECHNICAL REPORT AFAPL-TR-70-21

May 1970

Air Force Aero Propulsion Laboratory
Air Force Systems Command
Wright-Patterson Air Force Base, Ohio

FOREWORD

This report covers work performed on contract number F33615-67-C-1122, BPS 7(63-301201-62405214) during the period 15 November 1968 to 15 November 1969 at The University of Michigan. The work was sponsored by the Air Force Aero Propulsion Laboratory and the project monitor was Mr. W. Lee Bain. The project director was Professor J. A. Nicholls, Department of Aerospace Engineering, The University of Michigan. This report covers the research conducted in the last (third) year but includes some discussion of the earlier work for the sake of continuity. The progress for the first two years is reported in the following two reports;

1) LaPointe, C. W., "Supersonic Mixing and Combustion," (AFAPL-TR-68-12).
2) LaPointe, C. W., "An Experimental Study of Coaxial Turbulent Mixing of Liquid and Gaseous Fuel with Air," (AFAPL-TR-69-64).

The authors of this report would like to acknowledge the able assistance of Messers D. R. Glass, D. E. Geister, and W. J. Lane in effecting this experimental research.

This report was submitted to the Air Force on 18 February 1970.

Publication of this report does not constitute Air Force approval of the report's findings or conclusions. It is published only for the exchange and stimulation of ideas.

W. Lee Bain

W. Lee Bain
Air Force Aero Propulsion Laboratory
Wright-Patterson AFB, Ohio 45433

ABSTRACT

Turbulent mixing between coaxial streams of dissimilar gases is experimentally studied. The inner stream is tagged with a tracer molecule, hydrogen fluoride. Species concentrations and turbulent mixing extents are determined spectroscopically. Details of the technique for radiatively absorbing cold jets are given.

Experiments with cold jets at subsonic and transonic Mach numbers show that the mixing layer width increases with nondimensional mass flux difference, and decreases with increasing Mach number level.

Supersonic mixing and combustion of hydrogen and air is obtained using a three phase AC arc heater to heat the air. Schlieren photographs show a substantial increase in the rate of jet spread when combustion occurs. Preliminary determinations of temperature and concentration profiles, using the HF tracer, are presented.

TABLE OF CONTENTS

LIST OF TABLES

LIST OF ILLUSTRATIONS

NOMENCLATURE

$\bar{a}_\nu$	measured path integrated absorption
A	area
b	mixing layer width; also, spectral line half-width
$B_\nu(T)$	Planck black body function
C_p	constant pressure specific heat
d/dt	derivative following flow at its mean velocity
D/Dt	substantial derivative
e	efficiency
h	enthalpy
h_θ	chemical heat of formation
$I_\nu, \bar{I}_\nu$	spectral radiance, measured spectral radiance
k_ν	absorption coefficient
K	equilibrium reaction rate constant for hydrogen fluoride polymerization
ℓ, L	distance along spectral path, spectral path length
m	molecular weight
M	Mach number
p	power input to arc heater
P	pressure
r, R	radial distance, outer radius of jet
R, R_o	gas constant, universal gas constant
S	spectral line strength
t	time
T	temperature
u, v, w	velocity components in cartesian coordinates
U, V, W	transformed velocity components

U	axial jet velocity
w	flow rate
x, y, z	cartesian coordinates
X, Y, Z	transformed coordinates
Z	axial downstream distance in jet system
α	broadening effectiveness
γ	ratio of specific heats
ϵ	eddy viscosity
μ	spectral wavelength
ν	spectral frequency in wavenumber
$\delta\nu$	effective spectral slit width
ρ	density
ϕ	phase lag between pressure and density fluctuations, also equivalence ratio
ω	frequency of turbulent fluctuations

Subscripts

c	arc chamber condition
$\mathrm{C_L}$	jet system centerline
e	effective broadening pressure
f	chemically frozen flow
HF	hydrogen fluoride
i, j	denotes cartesian coordinates
i	incompressible; also, inside diameter of center jet injector tube
i, o	inner and outer jets
J	rotational quantum number
m	spectral line center
o	cold stagnation conditions

s	species
TG	test gas, N_2 or H_2, used in center jet
1/2	half-radius based on HF partial pressure
1, 2	individual streams in coflowing system
∞	conditions outside of turbulent mixing region

Superscripts

*	nozzle throat
'	turbulent fluctuations
$\bar{}$	averaged quantities in turbulent flow

I. INTRODUCTION

The need for noninterfering diagnostic techniques to investigate flows with compressible turbulent mixing and combustion is beyond doubt. Employment of specially cooled physical probes—chemical samplers, pitot tubes, thermocouples, hot wires—may be impossible, difficult, or subject to appreciable error in reacting flows. Flow field modification due to the probe's presence must be considered, especially in supersonic flows where unwanted shock waves result. Modification of density fields and density and pressure fluctuations by probes may severely limit experimental validity in compressible and reacting turbulent streams. When chemical composition is sought, the probe itself may affect the measurement. Recently, Sforza and Trentacoste[1] have raised many questions concerning the influence of probes in conventional turbulence experiments—even in subsonic incompressible flows. Spectroscopy offers an important alternate method of determining the chemical composition and thermodynamic state of a flow system.

A noninterfering infrared spectroscopic technique using hydrogen fluoride as a tracer molecule has been devised, built, and tested at The University of Michigan Gas Dynamics Laboratories. The technique is well-suited for application to fuel-air mixing situations. With measurements of absorption and emission of radiant energy from a free mixing jet system it is possible to determine the temperature and spatial extent

of the fluid which has been tagged with the spectrally active hydrogen fluoride tracer.

Hydrogen fluoride was chosen as the tracer gas for a number of reasons. It is a strong absorber in its fundamental vibration-rotation band centered at 2.5μ. The R-banch (Fig. 1) of this band extends into spectral regions devoid of atmospheric interference by CO_2 and H_2O, which are also common combustion products. The line spacing is such that a single line may be easily isolated with monochromators of moderate resolution. Spectral line strengths and shapes are known. Finally, its strong chemical bond allows its use at high temperature.

The investigations presented herein are a continuation of studies initiated by LaPointe[2, 3]. A complete description of the spectroscopic technique and apparatus necessary for hydrogen fluoride absorption experiments in cold jets is given in Ref. 3. In that reference LaPointe also presents the results of light scattering measurements when a center jet of water was used.

This report presents the results of an investigation wherein hydrogen fluoride infrared absorption spectroscopy was used to obtain concentration profiles and turbulent mixing layer widths of free coaxially mixing streams of hydrogen and nitrogen with air; also, free submerged air jets injected with hydrogen fluoride tracerwere examined at several axial positions. The data has been obtained in the subsonic and transonic

regimes. Furthermore, supersonic combustion of a submerged jet has been obtained using a three phase high pressure arc heater with a special plug nozzle that allows central injection of fuel (H_2) along with the hydrogen fluoride tracer into the arc heated air. These tests indicate that absorption and emission infrared hydrogen fluoride (HF) spectroscopy can be utilized to obtain temperatures in the reacting, supersonic flows. Chemical ignition and reaction times can thus be inferred from temperature data. Details of the experimental technique, apparatus, and completed investigations are described in the following sections. First, however, several important features of compressible turbulent mixing with and without combustion are presented.

II. THE EFFECT OF COMPRESSIBILITY AND COMBUSTION ON TURBULENT MIXING RATES

Knowledge of turbulent mixing rates associated with the spreading of submerged jets and the mixing of coflowing streams is of substantial importance to many combustion propulsion devices. In recent years it has become increasingly necessary to investigate the effects of compressibility and combustion on turbulent fuel-oxidizer mixing rates in ramjets, scramjets, and air-augmented rockets. Turbulent spreading rates encountered in rocket plumes and jet exhausts also depend on the same phenomena.

A. THE EFFECT OF COMPRESSIBILITY

Since Prandtl, eddy viscosity has been used as a measure of turbulent mixing rates, usually with good success for incompressible flows. Usually the eddy viscosity was assigned a constant value, or a value dependent solely on the cross stream derivative of the mean velocity. During the past two decades eddy viscosity expressions, modified for compressibility, have appeared in the literature. Schetz[4] lists several compressible eddy viscosity formulations.

To better understand compressible turbulent structure and predict the root mean square values of velocity, pressure, density, and temperature fluctuations, the concepts of vorticity, acoustic, and entropy modes have been introduced. Demetriades[5] indicates that dimensionless density

and temperature fluctuations are of the order of velocity fluctuations in heated compressible wakes. Most investigations into compressible turbulence point to the importance of density levels, gradients, and fluctuations. Laufer[6], using a coordinate transformation similar to those normally applied to compressible boundary layers, has succeeded in modifying the turbulent Reynolds stress for local values of density, its gradients and fluctuations. A summary of the method is presented.

The instantaneous mass and momentum conservation equations, i.e.

$$\frac{\partial \rho}{\partial t} + \frac{\partial \rho u_i}{\partial x_i} = 0 \tag{1}$$

$$\rho \frac{\partial u_i}{\partial t} + \rho u_j \frac{\partial u_i}{\partial x_j} = - \frac{\partial P}{\partial x_i} + \text{viscous stresses} \tag{2}$$

are transformed to the new coordinates:

$$X = x \tag{3}$$

$$\rho_\infty Y = \int^{y} \rho(x, y, z, t)\, dy \tag{4}$$

$$Z = z \tag{5}$$

It should be noted that the lateral coordinate is transformed using the instantaneous value of density rather than an averaged value. In the

transformed space the velocity components are selected so that conservation of mass is correspondingly satisfied, thus

$$U = u \tag{6}$$

$$\rho_\infty V = \rho v + \rho_\infty \frac{\partial Y}{\partial t} + U \frac{\partial Y}{\partial x} + W \frac{\partial Y}{\partial z} \tag{7}$$

$$W = w \tag{8}$$

Upon transformation the compressible conservation equations (Eq. (1) and (2)), assuming constant pressure and neglecting viscous stresses, take the incompressible form. Next, as ordinarily done in obtaining turbulent conservation equations, the velocities in the transformed space are "split" into average and fluctuating components. Subsequent averaging with boundary-layer-type approximations yields for planar flow

$$\frac{\partial \overline{U}}{\partial X} + \frac{\partial \overline{V}}{\partial \overline{Y}} = 0 \tag{9}$$

$$\frac{\partial \overline{U}^2}{\partial X} + \frac{\partial \overline{U}\overline{V}}{\partial \overline{Y}} = - \frac{\partial \overline{U'V'}}{\partial \overline{Y}} \tag{10}$$

Thus, the compressible conservation equations have been transformed into the turbulent incompressible form. The term, $\overline{U'V'}$, is the incompressible Reynolds stress. This procedure is valid provided the density-velocity correlation, $\overline{\rho'v'}$ is sufficiently small compared to $\overline{\rho}\overline{v}$, and pressure fluctuations are negligible.

Laufer[6] (using Eq. (6) and (7)) obtains the following expression for the compressible Reynolds stress in terms of the "incompressible" velocities:

$$-\overline{\rho u'v'} = -\rho_\infty \overline{U'V'} + \rho_\infty \left[\overline{U'^2} \frac{\partial \overline{Y}}{\partial x} + 2\overline{U}\,\overline{U' \frac{\partial Y'}{\partial x}} + \overline{U' \frac{\partial Y'}{\partial t}} + \overline{U'^2 \frac{\partial Y'}{\partial x}} + \overline{U'W' \frac{\partial Y'}{\partial z}} \right] \tag{11}$$

The first term in the bracket on the right of Eq. (11) indicates the dependence of compressible Reynolds stress on the longitudinal density gradient, while the remaining terms in the bracket indicate dependence on density fluctuations, since $\rho_\infty Y' = \int \rho' \, dy$. Furthermore, the compressible eddy viscosity coefficient can be expressed in terms of the incompressible coefficient plus corrections for density gradients and fluctuations. The effect of density level, alone, on eddy viscosity is observed by neglecting density gradients and fluctuations. A form similar to the Ting-Libby[7] compressible eddy viscosity coefficient is obtained, i.e.

$$\epsilon = \left[\frac{\rho_\infty}{\rho} \right]^2 \epsilon_i \tag{12}$$

Equation (12) is a first order correction to the incompressible eddy viscosity coefficient, ϵ_i, for flows of variable density.

The mixing rate of a turbulent shear layer may also be modified for density. The mixing rate, dependent on turbulent intensity and mean velocity, is usually written

$$\frac{b}{Z} \sim \frac{\sqrt{\overline{v'^2}}}{\frac{1}{2}(u_1 + u_2)} \tag{13}$$

and whenever possible, one tries to relate the rms value of the turbulent velocity fluctuations to the cross-stream mean velocity and density differences. For an incompressible flow, Prandtl's mixing length hypothesis gives

$$\sqrt{\overline{v'^2}} \sim \sqrt{\overline{u'^2}} \sim \ell \frac{\partial \bar{u}}{\partial y} \sim u_2 - u_1 \tag{14}$$

The corresponding eddy viscosity formulation, according to Prandtl, is

$$\epsilon = -\frac{\overline{u'v'}}{\frac{\partial \bar{u}}{\partial y}} \sim b(u_2 - u_1) \tag{15}$$

where it is assumed that $\overline{u'v'} \sim \overline{u'^2}$; that is, the cross correlation is proportional to the turbulent kinetic energy. As indicated in Eq. (11), neglecting the bracketed terms, the ratio of turbulent kinetic energies is inversely proportional to the corresponding density ratio, therefore

$$b \sim \frac{\rho_\infty}{\rho} b_i \tag{16}$$

for "similar" incompressible and compressible turbulent shear layers. The velocity levels, u_1 and u_2, of similar incompressible and compressible flows are identical. The incompressible mixing layer width, b_i, is given by Abramovich[8] as

$$\frac{b_i}{Z} = c \left| \frac{1 - \frac{u_1}{u_2}}{1 + \frac{u_1}{u_2}} \right| \tag{17}$$

where the constant, c, is equal to .27.

Thus, the growth rate of a compressible mixing layer is given as

$$\frac{b}{Z} = \frac{2c\,\rho_\infty}{(\rho_1 + \rho_2)} \left| \frac{1 - \frac{u_1}{u_2}}{1 + \frac{u_1}{u_2}} \right| \tag{18}$$

where the density term of Eq. (16) is written as an average density, $1/2\ (\rho_1 + \rho_2)$, of the mixing layer. The same procedure—with a corresponding resultant density dependence—can be applied to the case of a fully developed submerged jet. For a submerged jet the density ρ_∞, i.e. that outside of the turbulent shearing region, is set equal to ambient density; and therefore one expects a jet of light gas to spread faster than a jet of heavier gas of equal velocity. Recent studies by Abramovich et al[9]

indeed show increased spreading rates of jets of low molecular weight. By again examining Eq. (13) and (18), it can be concluded that compressible turbulent mixing rates are affected by three factors: (1) the velocity difference between the mixing fluids nondimensionalized with an average velocity; (2) the density level of the mixing region; and (3) the average value of the turbulent kinetic energy.

Recent studies show that compressibility also influences turbulent mixing through the acoustic fields generated by the flowing streams or jets. The density fluctuations and pressure fluctuations may couple to intensify the turbulent structure and extent. Glass[10], at The University of Michigan Gas Dynamics Laboratories, has clearly demonstrated the effect of acoustic radiation on the spreading rate of underexpanded jets. The nature of solid surfaces—acoustically absorptive or reflective—near the turbulent mixing region appear to be very important.

B. THE EFFECT OF COMBUSTION

Compressible turbulent mixing is further complicated by the addition of combustion. Combustion appears to enhance turbulent fluctuations and mixing rates. Furthermore, ignition delay and reaction times are influenced by the turbulent mixing. Wooldridge and Muzzy[11] have probed, with hot wires, the edges of a flame situated in a boundary layer. They have observed substantial increases in turbulent velocity fluctuation levels and a 40% increase in the boundary layer width when

compared to the nonreacting flow. Heyman, Sanderson, and Steel[12], utilizing a split shock tunnel, report increased mixing layer growth rates with combustion. Eschenroeder[13], has shown that turbulence is intensified by chemical heat release and Eschenroeder and Chen[14] have subsequently shown that eddy diffusivity is substantially increased. Their results depend on the phase relation between density fluctuations and chemical heat release (also expressible as a phase lag between density and pressure fluctuations), and in final form depend directly on $(\rho'/\rho)^2$. The concept of pressure-density phase coupling has been extended to the hydrogen-oxygen reaction in a mixing layer by Malte[15].

The intensification of turbulent kinetic energy by pressure and density fluctuations is first noted by examining the turbulent kinetic energy conservation energy. By following the procedure given by Hinze[16] this equation becomes, for a compressible flow

$$\frac{\overline{du'^2/2}}{dt} = -\overline{u_i'u_j'}\frac{\partial \bar{u}_i}{\partial x_j} - \overline{u_j'\frac{\partial u'^2/2}{\partial x_j}} - \overline{\frac{u_i'}{\rho}\frac{\partial P}{\partial x_i}} + \text{viscous terms} \qquad (19)$$

The term $d(\overline{u'^2}/2)/dt$ represents the rate of change of the average turbulent kinetic energy following the flow at its average velocity. The first term on the right represents the energy transferred from the mean motion through the turbulent shear stress, while the second term represents the convective diffusion by turbulence of the turbulent kinetic

energy. The last term on the right appears to be a pressure work term. Physically, it is the work per unit time per unit mass done by the pressure forces as seen by an observer moving at the average flow velocity. This term has special significance in chemically reacting turbulent flows. While all the terms of Eq. (19) are influenced by combustion through its effect on turbulent velocity fluctuations, only the pressure work term indicates the source of additional turbulent kinetic energy added by combustion.

A form of the pressure work term that clearly shows the coupling between pressure and density fluctuations is now derived. Consider a fluid particle in a turbulent flow: an observer moving at a constant average flow velocity will only detect changes in the turbulent kinetic energy of the particle. Then the mechanical energy conservation equation as given by Liepmann and Roshko[17] becomes

$$\frac{D\, u_i'^2/2}{Dt} = -\frac{u_i'}{\rho}\frac{\partial P}{\partial x_i} \tag{20}$$

The change in energy of the fluid element as it travels during time t_1 to t_2 is

$$\Delta u_i'^2/2 = -\int_{P(t_1)}^{P(t_2)} \frac{dP}{\rho} \tag{21}$$

and the average power delivered to the turbulent field during time Δt is

$$\frac{\Delta u_i'^2/2}{\Delta t} = -\frac{1}{\Delta t}\int_{P(t_1)}^{P(t_2)} \frac{dP}{\rho} \tag{22}$$

For a flow field with constant average pressure, Eq. (22) can be written in terms of density and pressure fluctuations

$$\frac{\Delta u_i'^2/2}{\Delta t} = \frac{1}{2t}\int_{P'(-t)}^{P'(t)} \frac{\rho' dP'}{\bar{\rho}^2} \tag{23}$$

The equation is valid to first order in density fluctuations; and the fluid particle is observed for one fluctuation cycle.

If the fluctuation period 2t is much less than the residence time (of the observer in the turbulent reacting field) then an ensemble average of fluid particles at one point in the flow field gives the rate of change of average turbulent kinetic energy due to pressure-density coupling as

$$\overline{\frac{du_i'^2/2}{dt}} = \overline{\frac{1}{2t}\int_{P'(-t)}^{P'(t)} \frac{\rho' dP'}{\bar{\rho}^2}} \tag{24}$$

For chemical nonequilibrium Eq. (24) is nonzero. For sinusoidal fluctuations Eq. (23) can be easily integrated. Eschenroeder[13] gives the power delivered to the fluctuating field as

$$\frac{\omega}{2\bar{\rho}^2} P'\rho' \sin\phi$$

The phase difference, ϕ, between density and pressure fluctuations is determined from the chemical kinetics.

The power added to the turbulent kinetic energy by chemical heat release from the hydrogen-oxygen reaction is given in Ref. 15. The chemical kinetics is introduced using the global reaction times of Cohen[18], and the pressure and density fluctuations are related by an acoustic type equation. The resulting expression for turbulent kinetic energy increase is

$$\frac{d\,\overline{u_i'^2/2}}{dt} = T\,\frac{d\,H_2O}{dt}\,h_\theta\,\frac{m_{H_2O}\,R\,\gamma_f}{P\,C_p}\left[(\gamma_f - 1)\,\frac{1800}{T} + 1.7\,\gamma_f\right]\frac{\overline{\rho'^2}}{\bar{\rho}^2} \qquad (25)$$

Thus the intensification of turbulence by combustion is principally proportional to the amount of heat release and the density fluctuations. Modification of turbulent mixing rates for reacting flows must consider the effect of both variable density and intensified turbulent kinetic energy.

III. THE HYDROGEN FLUORIDE TRACER MOLECULE INVESTIGATIVE TECHNIQUE

As indicated hydrogen fluoride tracer molecule spectroscopy has the potential of determining the thermodynamic state and spatial extent of a fluid which has been tagged with the tracer. The necessary experimental technique and setup for spectroscopically examining jets using HF absorption is presented in detail by LaPointe[3]. Consequently, only a brief description of pertinent apparatus and HF spectroscopy is presented here. The apparatus necessary for supersonic combustion experiments using HF tracer is also discussed. Emission-absorption spectroscopic methods that can be utilized to investigate reacting jets are presented.

A. THE BASIC EXPERIMENTAL SETUP AND PROCEDURE

A physical schematic of the optical apparatus is shown in Fig. 2. The infrared source is a tungsten horizontal filament lamp (GE 18A/T10/2P-6V, SR-6A filament) which is mounted so that the filament is vertical and imaged on the median plane of a vertical coaxial mixing jet system. The beam is subsequently re-focussed on the entrance slit of a grating monochromator. Spectral scanning is accomplished by rotating the grating with a synchronous motor. The monochromator is a Perkin-Elmer Model 98G fitted with a grating blazed at $\lambda = 2.5\mu$. For HF (hydrogen fluoride) tests, allowed scanning is from 1.6 to 2.75μ, with entrance slit width set at 70μ. A long wave pass filter screens out

unwanted higher order diffraction beyond 1.6μ. Spectral radiance which has been dispersed by the grating is detected by a Kodak Ektron Type N photoconductivity cell (lead sulfide, PbS, cell) after undergoing six-power demagnification. System focal length is 36, limiting aperture is 3 in.

The light beam is chopped at 100 Hz with a resulting waveform of trapezoidal shape. For absorption experiments of cold jets the chopper is located immediately after the light source. In combustion experiments the chopper is located immediately before the monochromator slit, so that both light source and flame radiation are chopped. The resulting 100 Hz PbS detector signal and a 100 Hz reference signal of trapezoidal waveform are applied to the input of a P.A.R. Model 120 lock-in-amplifier. The lock-in-amplifier detects at 100 Hz with a 10 Hz bandwidth. The amplitude of the chopped PbS signal conveys the necessary spectral data and whatever noise is contained within the 10 Hz bandwidth centered on 100 Hz. To further eliminate noise in supersonic combustion experiments employing the arc heater, the PbS cell signal is preamplified at the monochromator. All data is monitored in a control room adjacent to the test cell. The toxic nature of hydrogen fluoride and safety precautions in arc heater operation make this necessary.

In the present setup hydrogen fluoride, alone and premixed with test gas, forms the inner jet of a vertical coaxial jet mixing system. Premixing occurs

at an ejector located several feet upstream of the nozzle exit. The center jet of the ejector, which consists of test gas, is choked to low pressure supersonic flow, so that it can mix with the gaseous HF. The hydrogen fluoride is supplied at 20 to 30 psia by heating an immersed cylinder of anhydrous liquid HF in a water bath at 100°F. (The boiling temperature of HF at 1 atm is 67°F.) Hydrogen fluoride is a very corrosive substance; monel and copper are used exclusively in the plumbing. Special materials are necessary in transducers used to monitor flow rate and pressure, also sealed chromel alumel thermocouples have withstood its corrosive nature. To utilize the tracer nature of HF its partial pressure in the inner jet is kept below 5%. Heating tapes are wrapped around the separate HF and test gas pipes to prevent condensation. Once the HF and test gas are mixed, condensation of HF due to the subsequent low temperatures is eliminated, because the inclusion of foreign gas in effect causes the HF to supersaturate.

The jet mixing test stand for absorption experiments with optical platform is shown in Fig. 3. For supersonic combustion experiments the optical platform is suspended above the arc heater. The premixed test gas—HF composite becomes the inner jet of a coaxially mixing system using an outer air jet. (This is also true in the supersonic combustion experiments.) Two modes of turbulent mixing are obtained.

In the near region where the respective jet cores exist, the mixing layer between inner and outer coaxially mixing streams may be examined. Once the two initial jets are mixed, the resulting flow may be treated as a submerged jet. In either case the monochromator is set at the peak of the desired HF absorption spectral line. Transverse absorption (also emission in the combustion case) profiles are obtained by translation of the optical platform. Table movement is maintained using a synchronous motor, and position detection is accomplished with a servo system. Vertical position is set manually. Spectral output, at one wave number, is displayed on an x-y recorder, while spectral scans in wave number are displayed on an x-t recorder.

The flow rate of the inner jet gas, nitrogen or hydrogen in completed investigations, is measured by a rotometer, while the hydrogen fluoride flow rate is monitored by an orifice meter and its value calculated using LaPointe's[3] HF mass flow equation. The temperature of the HF-test gas mixture is measured by a thermocouple located 1 ft upstream of the nozzle exit and 2 ft downstream of the ejector. For subsonic jets the nozzle exit pressure is equal to atmospheric pressure; the necessary flow parameters at the nozzle exit are then calculable. By assuming that the hydrogen fluoride is a perfect gas and that it has mixed completely with the test gas, the inner jet exit velocity becomes

$$U = \frac{R_o T}{PA}\left[\frac{w_{HF}}{m_{HF}} + \frac{w_{TG}}{m_{TG}}\right] \tag{26}$$

and its density is determined from

$$\rho = \frac{w_{TG} + w_{HF}}{UA} \tag{27}$$

The area, A, is that of the inside of the inner jet injector tube. The speed of sound is calculated assuming $\gamma = 1.4$ (that for diatomic molecules without vibration) and the Mach number is determined. The flow rate of the outer air jet is measured by an orifice meter; its stagnation temperature is also measured. Thus, for subsonic expansion to atmospheric pressure, its flow parameters are easily determined.

B. SUPERSONIC COMBUSTION EXPERIMENTAL APPARATUS AND PROCEDURE

To apply the hydrogen fluoride tracer molecule technique to supersonic turbulent mixing with combustion, the previously described experimental setup, modified for emission spectroscopy, is utilized with a high pressure three phase AC arc heater system capable of generating gas temperatures to 5000^{o}K. The arc heater chamber is surrounded by magnetic coils; the resulting magnetic field causes the arc to continuously rotate about the circular electrodes contained within the chamber. Electrode failure is thereby reduced. A complete description of the arc heater

and its performance is given by Geister[19]. The exit nozzle of the arc heater is of plug type. A photograph of the arc heater with magnetic coils and plug nozzle is shown in Fig. 4.

The supersonic plug nozzle has the advantage of allowing a central region where a fuel-hydrogen fluoride mixture can be injected (at subsonic or sonic velocity) into the hot arc heated supersonic air stream. The plug nozzle bottom section with conical plug and necessary plumbing is shown in Fig. 5. Figure 6 shows a top view of the plug nozzle with top section in position about the conical plug. The findings of Krull and Beale[20, 21] were employed in the plug nozzle design; to ease design and construction a conical plug was chosen. All parts of the plug nozzle are made of 99. 9% oxygen free hard copper. The high heat transfer rates of copper insured sufficient cooling; also, as previously indicated copper is capable of withstanding the corrosive nature of HF. The outer surfaces of the plug nozzle (as well as those of the arc heater chamber) are cooled by water circulating in copper tubes. The conical plug, with hollow center, and its support are also water cooled. Within the hollow conical plug is located a vertical tube for fuel-HF transport and injection.

The nozzle throat for the arc heated air stream is formed between the cone and the lip of the top section - as shown in Fig. 6. The throat area is 0. 066 sq. in. The injector tube i. d. is 0. 300 in. and the diameter of

the outer lip is 0. 648 in. ; also, the cone included angle is 72^{o} and it extends 0. 190 in. above the nozzle throat to form the supersonic part of the plug nozzle. Expansion of the arc heated air to ambient pressure is primarily accomplished by a Prandtl Meyer expansion centered at the nozzle lip. At arc chamber pressures from 60 to 200 psig, expansion to Mach numbers from 1. 7 to 2. 4 is obtained. With the plug nozzle typical air flow rates are between 0. 05 and 0. 15 lbm/sec; arc chamber temperatures are 1500^{o}K to 3000^{o}K.

Completed investigations have used hydrogen as the fuel in the inner jet; its flow rate with tracer amounts of HF can be varied between 0. 001 and 0. 012 lbm/sec. The equivalence ratio, ϕ, the fuel to oxidizer ratio divided by the stoichiometric fuel to oxidizer ratio, based on overall H_2 and air flow rates,has the range from fuel lean, 0. 4, to fuel rich, 6. 0. Arc chamber conditions sufficient for auto-ignition of hydrogen and oxygen in the free mixing jet system are maintained. Flow rates are monitored using a rotometer for the inner jet, and orifice meters for the outer arc heated air jet and hydrogen fluoride tracer. Hydrogen fluoride is supplied to and "premixed" with the inner jet gas as previously described.

It is important to determine nonmeasureable flow parameters accurately and quickly. The arc chamber enthalpy can be calculated knowing its pressure, electrical power input, and energy loss due to cooling. The

energy drawn from the hot gases by the cooling water is determined by measuring the water temperature, in the separate cooling lines, before and after cycling through the arc heater and nozzle. However, for supersonic flow, an approximate method that does not require knowledge of cooling water temperatures can be used. It relies on a modified real gas—sonic flow relation derived by Winovich[22] for arc heater enthalpies between 1000 and 10,000 Btu/lbm and pressures between 1 atm and 100 atm. The formula is

$$\frac{w}{A^* P_c} = \frac{.133}{h_c^{.4}} \tag{28}$$

where

w = arc heater flow rate, lbm/sec
A^* = arc heater nozzle throat area, in.^{2}
P_c = arc heater chamber pressure, psia
h_c = arc heater enthalpy, Btu/lbm

Since the flow velocity in the arc chamber is low, its conditions are taken as stagnation values. The enthalpy of the arc heated gas is proportional to the effective power input and inversely proportional to the flow rate, i. e.,

$$h_c = 947 \frac{pe}{w} \tag{29}$$

where

p = power input, megawatts

e = efficiency, decimal fraction.

The troublesome quantity to measure is the efficiency. Its value may be inferred from measurements of arc chamber pressure and temperature with cold flow through the chamber without the arc operating. Then the ideal mass flow formula[23] for air holds, i. e. ,

$$\frac{w}{A^* P_o} = \frac{.532}{\sqrt{T_o}} \tag{30}$$

where T_o is the stagnation temperature of the cold air in ^oR. The effective power input to the arc heated gases can be found by combining Eq. (28), (29) and (30) to give

$$pe = \left[\frac{P_c}{P_o}\right]^{2.5} \frac{T_o^{1.25} w}{30300} \tag{31}$$

Thus, by knowing the flow rate, the hot arc chamber pressure, and the arc chamber pressure and temperature without the arc operating, one can determine pe and calculate an average chamber enthalpy from Eq. (29). An average chamber temperature can be inferred using real gas tables for air.

The supersonic air flow conditions are found assuming perfect expansion to ambient pressure and frozen flow. Exit conditions—velocity, density, temperature—of the cold inner jet can be ascertained only if this

jet expands to ambient pressure before mixing and its resultant area or Mach number is determinable. In tests conducted with arc chamber pressures of 180 psig and hydrogen "K" bottle regulator pressures of 50 psig, the outer air jet caused the inner H_2 jet to be contracted inward. Since the condition occurred within a short distance from the nozzle exit, turbulent mixing is negligible. This flow configuration is taken as indicative of sonic conditions in the inner jet; the pressure is assumed equal to ambient and the other important flow parameters are calculable.

The experimental procedure for supersonic combustion tests is now described. A low flow rate of air is maintained through the arc chamber without the arc operating; the center jet with a mixture of nitrogen and hydrogen fluoride is initially used to find the desired HF spectral line and to measure the HF flow rate. The arc is then turned on and the flow rate increased until the desired arc chamber pressure is obtained. At this point the hydrogen, being at higher bottle regulator pressure than the nitrogen, is turned on by activating its solenoid valve; the nitrogen valve is then closed. The arc heater is operated "at pressure" for one minute, during which time combustion occurs and the desired Schlieren photographs and HF spectral measurements are made. To cease operation, the H_2 is first replaced with N_2 in the center jet, then the arc heater is turned off. A schematic of the complete experimental apparatus necessary for these investigations is presented in Fig. 7.

C. SPECTROSCOPIC MEASUREMENT

The necessary hydrogen fluoride spectroscopy and subsequent data reduction methods are now presented. The system geometry—light source, jet, monochromator—is shown in Fig. 8. For nonhomogeneous radiatively absorbing cold gases the equation of radiative transfer gives the measured path integrated absorptance as

$$\bar{a}_\nu(y) = \frac{1}{\delta\nu} \int_{\delta\nu} \left\{ 1 - \exp\left[- \int_0^L P k_\nu d\ell \right] \right\} d\nu \qquad (32)$$

where

P = partial pressure of spectrally absorbing species, atm
k_ν = absorption coefficient, $atm^{-1} cm^{-1}$
ν = frequency in wave number, cm^{-1}
$\delta\nu$ = effective spectral slit width of monochromator, cm^{-1}
L = path length, cm
y = cross jet coordinate

As shown by LaPointe[3], $\bar{a}_\nu(y)$ defined by Eq. (32) is the peak or spectral centerline value of the measured absorptance. The rationale for setting the monochromator at the peak of the measured absorption spectral line and spatially scanning the jet system in the y direction is thus indicated. Due to the cylindrical symmetry of the coaxial jet system, the profiles of the path integrated absorptances obtained from the experiments, i. e., $\bar{a}_\nu(y)\ \delta\nu$, are Abel transformed to give the radial dependences of the

spectral variables contained within the exponential of Eq. (32). Depending upon the value of the path integrated absorptance, the data can be reduced by weak line or strong line approximations. Also, a technique valid in the intermediate region between weak and strong line regimes, that only assumes constant spectral line half-width, has been devised and utilized.

If the integral of the exponential in Eq. (32) is sufficiently small, the following approximation is valid

$$\bar{a}_{\nu}(y)\delta\nu = \int_{\text{line}} \left[\int_{o}^{L} P k_{\nu} d\ell \right] d\nu \tag{33}$$

Integration is performed over the spectral line width instead of the effective slit width, since $\delta\nu \gg b$. The parameter, b, is the spectral line half-width at half-height and is expressed in wavenumbers, cm^{-1}. The spectral line shapes of diatomic hydrogen fluoride, with fundamental vibration-rotation radiation being in the infrared, are given by the Lorentz contour formula, i. e. ,

$$k_{\nu} = \frac{S}{\pi} \frac{b}{b^2 + (\nu - \nu_m)^2} \tag{34}$$

where

ν_m = spectral line center wavenumber

S = spectral line strength, $atm^{-1}cm^{-2}$

The line strength is defined as

$$S = \int_{\text{line}} \dot{k}_{\nu} \, d\nu \tag{35}$$

With Eq. (35), the weak line approximation for the measured absorption becomes

$$\bar{a}_{\nu}(y)\delta\nu = \int_{0}^{L} PS_{J} d\ell \tag{36}$$

The subscript J denotes the rotational quantum number of the examined spectral line in the R-branch of the fundamental vibration-rotation band of diatomic hydrogen fluoride. Values of the HF line strengths, S_J, are given by LaPointe[3] for rotational quantum numbers J = 0 to J = 8 in the temperature range 100^{o}K to 400^{o}K.

The Lorentz broadening, being dependent upon molecular collisions, is the only important mode of spectral line broadening for infrared radiation in cold gases. At higher temperatures, as in the supersonic combustion experiments, Doppler broadening due to thermal velocity should be considered. A combined spectral line profile due to Lorentz and Doppler broadening, called the Voight profile[3], can be utilized.

The strong line approximation, with only Lorentz broadening present, is now discussed. The integral of the exponential in Eq. (32) must be sufficiently large; the direct result of this requirement is that b^2 can be

neglected compared to $(\nu - \nu_m)^2$ in the denominator of the Lorentz contour formula given by Eq. (34). Then, Eq. (32) may be integrated with respect to ν; one obtains the following strong line formula

$$\bar{a}_\nu(y)\,\delta\nu = 2\sqrt{\int_0^L PS_J b\,d\ell} \qquad (37)$$

Abel transformation of the experimentally obtained spatial contours of $\bar{a}_\nu(y)\,\delta\nu$ yields, respectively point values of PS_J or $PS_J b$ for the weak or strong line cases. For data reduction of absorptances in the strong line region, the value of the spectral line half-width, b, must be determinable. These values have been obtained by LaPointe[3] for temperatures from 100°K to 400°K by using a resonant dipole-billiard ball approximation applied to HF by Simmons[24]. LaPointe[3] presents plots of b/P_e, where P_e is the effective broadening pressure, i. e. ,

$$P_e = \sum_s \alpha_s P_s \qquad (38)$$

The broadening effectiveness, α_s, of foreign gases N_2 and H_2 is given by Simmons[24] for hydrogen fluoride. By definition, the self broadening effectiveness, α_{HF}, is equal to unity. For J = 0 the values of α_s for nitrogen and hydrogen are respectively, 0. 20 and 0. 18. Both approach asymptotic values at J = 4, the respective values being 0. 10 and 0. 06 for nitrogen and hydrogen. The value of α_s for air is assumed equal to that for nitrogen.

Moreover, the half-widths of several HF spectral lines are practically constant when HF is used as a tracer in cold jets. This fact is utilized in the data reduction.

For hydrogen fluoride spectral lines defined by the Lorentz profile, Eq. (34), the measured absorptance, Eq. (32), can be rearranged in the following series if the half-width, b, is assumed constant:

$$\bar{a}_\nu(y)\delta\nu = 2\sum_{n=1}^{\infty}\left\{\frac{(-1)^{n+1}}{n!}\left[\int_0^L \frac{PS_J b}{\pi}\,d\ell\right]^n \int_0^\infty \frac{d(\nu-\nu_m)}{b^2+(\nu-\nu_m)^2\,n}\right\} \quad (39)$$

Integrations with respect to path length, ℓ , and spectral wavenumber, ν, have been separated. Term by term integration yields

$$\bar{a}_\nu(y)\delta\nu = \int_0^L PS_J d\ell\left\{1+\sum_{n=2}^{\infty}(-1)^{n-1}\left[\int_0^L \frac{PS_J}{\pi b}\,d\ell\right]^{n-1}\prod_{q=2}^{n}\frac{2q-3}{2q-2}\right\} \quad (40)$$

Equation (40) is plotted in Fig. 9. The integral $\int_0^L (PS_J/\pi b)d\ell$ is equal to the integral of the exponential in Eq. (32) evaluated at the spectral line center, i. e., at $\nu = \nu_m$. For $\int_0^L (PS_J/\pi b)d\ell$ approaching zero Eq. (40) takes the form of Eq. (36), the weak line approximation ; while for sufficiently large values of the integral Eq. (40) must approach the strong line condition for constant spectral line half-width, i. e. ,

$$\bar{a}_\nu(y)\delta\nu = \int_0^L PS_J d\ell \left\{ \frac{2}{\sqrt{\pi}} \left[\int_0^L \frac{PS_J}{\pi b}\, d\ell \right]^{-1/2} \right\} \tag{41}$$

Eq. (40) may be rearranged and thereby simplified for spectroscopic measurements in the weak line and intermediate regions extending up to the beginning of strong line validity. The resulting approximate equation

$$\int_0^L PS_J d\ell \cong \frac{\bar{a}_\nu(y)\delta\nu}{1 - .080 \dfrac{\bar{a}_\nu(y)\delta\nu}{b}} \tag{42}$$

with its useful range being

$$0 \leq \int_0^L \frac{PS_J}{\pi b}\, d\ell = \frac{4.08\, \bar{a}_\nu(y)\delta\nu}{12.84b - \bar{a}_\nu(y)\delta\nu} < 3$$

Average values of $\bar{a}_\nu(y)\delta\nu$ and b for investigations reported in Section III, are respectively 0.25 cm^{-1} and 0.07 cm^{-1}. Thus, the effect of line half-width in Eq. (42) is that of a first order correction to the weak line approximation. Therefore, some latitude in its accuracy is acceptable. Most of the jet absorption experiments reported in Section III are analyzed using Eq. (42); in most cases the variations in spectral line half-widths across the jet system are less than 20%.

To reduce the Abel inverted results to HF partial pressure or number density profiles, the temperature must be known so that S_J is determinable. Temperature may be inferred from core conditions of the jets or determined from a ratio technique using two spectral lines[3]. However, it is often easier to examine the J = 3 and J = 4 spectral lines of the HF R-branch, since the corresponding values of S_J are practically insensitive to temperature for $200^{o}K \leq T \leq 400^{o}K$.

The resulting HF partial pressure or number density profiles are nondimensionalized with their core or centerline value. Finally, the HF concentration profiles are assumed equal to corresponding profiles of the test gas with which the HF was premixed, since the turbulent motions are assumed to make no distinction between gas type and molecular diffusion is negligible. Thus the fraction of inner jet test gas to hydrogen fluoride based on number density is assumed constant across the mixing region.

In hot and reacting flows induced and spontaneous emission of radiation from the spectrally active gases - hydrogen fluoride in infrared region - is also present. For a nonscattering medium in local thermodynamic equilibrium the equation of radiative transfer, after integration along a straight path, becomes

$$I_\nu = I_\nu^{o} \exp\left[-\int_0^L \rho k_\nu d\ell \right] + \int_0^L \rho k_\nu B_\nu(T) \exp\left[-\int_0^L \rho k_\nu dx \right] d\ell \qquad (43)$$

where I_ν^o is spectral radiance from the source and $B_\nu(T)$ is the black body radiance, ρ is the density of spectrally active species. One is interested in isolating the black body radiance term at one wavelength, so that temperature may be calculated. As shown by Simmons[25], this is done in emission - absorption pyrometry of isothermal hot gases, and may be extended to nonhomogeneous regions by numerical procedures. Three measurements of spectral radiance are made: source alone, gas alone, and gas plus source. The method is utilized in the visible and infrared regions and it is relatively simple. Besides temperature it also provides a measurement of emissivity from which the density of the spectrally active species can be determined. That is, for an isothermal radiator the emissivity and absorptance are equal, and consequently the density can be determined from

$$\bar{a}_\nu = \frac{1}{\delta\nu} \int_{\delta\nu} \left\{ 1 - \exp\left[- k_\nu \rho L \right] \right\} d\nu \qquad (44)$$

Procedures using emission detection only, i. e., without using a light source, can be employed. Again due to the cylindrical symmetry of the jet system, the Abel inversion can be utilized. For the case of a thin gas, i. e., weak line approximation valid, with no light source present the measured spectral radiance is expressed as

$$\bar{I}_\nu(y) = \frac{1}{\delta\nu} \int_0^L \rho S_J B_\nu(T) d\ell \qquad (45)$$

With measured profiles of $\bar{I}_\nu(y)$, Eq. (45) can be Abel inverted, following the procedure of Ref. 3, to give point values of $\rho S_J B_\nu(T)$ as a function of radial position, i. e. ,

$$\rho S_J B_\nu(T) = -\frac{\delta\nu}{\pi} \int_r^R \frac{d\bar{I}_\nu(y)}{dy} (y^2 - r^2)^{-1/2} \, dy \qquad (46)$$

R is outer radius of the spectrally active cylindrical jet. Hydrogen fluoride line strengths of interest for combusting flows are given by Simmons[24]. Since the Planck black body function, B_ν, and HF line strength, S_J, are known functions of temperature and spectral wavelength, measurements of $\rho S_J B_\nu$ at two different wavelengths and subsequent ratioing should yield temperature determination; the density of the spectrally active HF is then calculable.

IV. TURBULENT MIXING IN COLD JETS INVESTIGATED USING HYDROGEN FLUORIDE ABSORPTION

Hydrogen fluoride absorption spectroscopy has been applied to determine concentration profiles and turbulent mixing rates in cold, nonreacting, subsonic and transonic free axisymmetric jets. The configuration for the jet system is shown in Fig. 10. In one series of experiments inner jets of nitrogen and hydrogen, premixed with tracer amounts of hydrogen fluoride, have been examined while coaxially mixing with an outer air jet. Attention was centered on the mixing layer between the inner and outer jet cores: the use of physical probes in this region may be restricted due to the narrow mixing layer extent and the proximity of nozzle surfaces.

The growth rate of mixing layers between parallel streams and in the initial regions of submerged jets is influenced not only by streamwise velocity differences and density levels but also by free stream turbulence and the wake formed from the initial boundary layers. Such mixing rates are difficult to theoretically analyze; also, local solid surface configurations peculiar to the device, e.g. combustor, may have a substantial influence on mixing. The effect of molecular weight on turbulent mixing can be discerned by comparing similar nitrogen and hydrogen mixing layers; this may be important in the mixing and combustion of air with low molecular weight H_2 fuel.

A further investigation used pure hydrogen fluoride centrally injected into subsonic air jets. The spreading rate of hydrogen fluoride was examined by observing concentration profiles at several axial positions in the turbulent air jet. A typical wave number scan of HF absorption showing several lines of the R branch of diatomic HF is presented in Fig. 11.

Before discussing the experimental results for the turbulently mixing jets, a brief description of the state of the gaseous hydrogen fluoride is necessary. Its state and subsequent molecular weight depend on the method of delivery and its temperature and partial pressure. The hydrogen fluoride, being in vapor form near its boiling point, is probably not a perfect gas. Most likely the hydrogen fluoride exists as a mixture of monomer and polymers. If the hydrogen fluoride is used as a tracer, and subsequently its partial pressure in the inner jet is kept below 5%, the errors resulting from its molecular weight determination and assumption of perfect gas are of minor influence on flow parameters as determined by Eq. (26) and (27). However, for meaningful spectroscopic measurements it is important to form some conclusions on the state of the hydrogen fluoride vapor. Up to this point the chemical symbol, HF, has been used interchangeably with the words hydrogen fluoride; in the remainder of the presentation (except for equations) the symbol HF will represent the diatomic hydrogen fluoride monomer, the complete vapor will be designated as hydrogen fluoride.

As previously stated, anhydrous hydrogen fluoride is heated in its cylinder to approximately $100^{o}F$, sufficient for a vapor pressure of 25 psia, as given by Ref. 26. During experiments, initial opening of the hydrogen fluoride flow valve resulted in a white, fuming, hydrogen fluoride condensate entering the jet system. However, after a short time, the clear hydrogen fluoride vapor began to flow, replacing the condensate. It is reported by Simons[27] that hydrogen fluoride vapor is in a polymerized state; for thermodynamic purposes the HF monomer may be considered in equilibrium with its hexomer, i.e.

$$6HF \rightleftharpoons H_6F_6$$

Simons results are based on vapor density measurements; the apparent molecular weight of the polymerized "perfect gas" can be determined from the reaction rate constant. As given by Simons

$$\log_{10} K = \frac{40,000}{4.579T} - 43.145 \tag{47}$$

where the equilibrium reaction rate constant, K, is related to monomer partial pressure by

$$KP^5 = \frac{1 - \frac{P_{HF}}{P}}{\left[\frac{P_{HF}}{P}\right]^6} \tag{48}$$

The temperature, T, is expressed in ^{o}K and the pressure and reaction rate constant are expressed in millimeters of mercury. The molecular weight of the vapor is determined using Eq. (47) and (48), with the assumption that the individual species HF and H_6F_6 are both perfect gases.

For typical conditions of hydrogen fluoride vapor in the heated cylinder, i.e. $T = 100^{o}F$ and P = 25 psia, Eq. (47) and (48) give $KP^5 = 3.6$. The apparent molecular weight, based on Simons' work, is 50; the fractional monomer partial pressure is 0.7. Once the hydrogen fluoride is mixed with the nitrogen or hydrogen gas, its partial pressure is reduced to a few percent. Thus, if residence times are sufficient, the hydrogen fluoride should exist mainly as monomer HF with a molecular weight of 20 at the nozzle exit. The following table presents data obtained during the mixing layer studies; it shows the appropriate hydrogen fluoride pressures in the core of the inner jet. The two cases presented used different test gases and different HF spectral lines; the temperature levels represent the maximum variation that occurred in the mixing layer experiments. The hydrogen fluoride partial pressure based on flow rate was determined using the following equation

$$\frac{P_{HF}}{P} = \frac{\frac{w_{HF}}{\bar{m}_{HF}}}{\frac{w_{TG}}{\bar{m}_{TG}} + \frac{w_{HF}}{\bar{m}_{HF}}} \tag{49}$$

Table 1. Typical Hydrogen Fluoride Partial Pressures in Jet Core

Quantum number, J	0	4
Test gas	N_2	H_2
Test gas flow rate; lbm/sec	.0193	.0089
Hydrogen fluoride pressure in core, spectroscopic measurement; atm	0.020	0.008
Core temperature; ^{o}R	540	440
Molecular weight based on spectroscopically measured pressure and equilibrium	20	20
Hydrogen fluoride flow rate; lbm/sec	0.0019	0.0016
Cylinder temperature; ^{o}F	100	110
Cylinder pressure; psia	27.0	27.2
Molecular weight of vapor in cylinder	50	50
Hydrogen fluoride partial pressure based on flow rate and molecular weight of 20; atm	0.12	0.02
Hydrogen fluoride partial pressure based on flow rate and molecular weight of 50; atm	0.05	0.01
Monomer partial pressure based on flow rate and molecular weight of 50; atm	0.035	0.007

The measurements listed in Table 1 indicate that the hydrogen fluoride is chemically frozen at the unmixed composition, i.e. corresponding to heated cylinder conditions, and that spectroscopically only HF monomer is detected. There is significant disagreement between spectroscopic measurements and measurements based on a molecular weight corresponding to HF monomer, thus indicating the presence of polymerization in the core flow. The value of the spectroscopically measured partial pressure is closest to that of HF monomer partial pressure based on flow rate with frozen composition, i.e. hydrogen fluoride molecular weight of 50 with a monomer partial pressure of 70%. Furthermore, the inclusion of foreign gas prevented the hydrogen fluoride from condensing at low temperatures below its atmospheric boiling point.

Nondimensional HF partial pressure profiles are presented in Fig. 12 to 17 for mixing layers between nitrogen and air jets; Fig. 18 to 21 show mixing between hydrogen and air jets. The Mach numbers of the nitrogen and hydrogen jets were varied from 0.3 to 0.9, while the outer air jet Mach number was varied from 0.3 to 1.1. The light beam was centered 0.59 in. downstream from the nozzle exit; the radius of the inner jet injector tube (3/8 in. o.d.) was 0.156 in. HF partial pressure profiles have been obtained assuming a linear temperature variation between the known inner and outer jet core conditions. Experimentally obtained path

integrated absorptances were Abel inverted using the constant spectral line half-width method, and the strong line approximation where necessary. Spectral line half width was determined from temperature and flow rate measurements of the hydrogen fluoride and test gas. The fractional number density of HF monomer to that of the nitrogen or hydrogen test gas is assumed constant across the mixing layer. Thus, the turbulent mixing is assumed to treat the hydrogen fluoride and the test gas equally, and the hydrogen fluoride is assumed to be chemically frozen with respect to polymerization. The HF profiles can be treated as concentration profiles of nitrogen or hydrogen.

The concentration profiles all exhibit the same general shape; through most of the mixing layer the decrease in partial pressure is linear. As shown by Abramovich[8] one expects a linear decrease in concentration, or add-mixture, through subsonic mixing layers. Near the outer edge of the mixing layer a more gradual-somewhat asymptotic-approach to the outer air conditions is noted. Profiles obtained at like flow conditions were slightly higher valued for the J = 0 HF spectral line than for the J = 4 line. This is an apparent effect probably resulting from minor data reduction or spectroscopic approximations.

The inner jet core is taken to exist from the jet system centerline to the point where the partial pressure profile begins to drop-off rapidly, indicating the start of the mixing layer. Some scatter is seen to occur in

the values of HF partial pressure measured in the core. Also, the centerline value of partial pressure is somewhat depressed from the value at the core edge. The maximum value of HF partial pressure generally exists at the point which is taken to be the core edge. This value gave the best results for nondimensionalization of the profiles; furthermore, it is a logical choice since it is desirable to eliminate core scatter from the mixing layer study. The peak in the profiles, at the core edge, is felt to be a real effect; it is not an apparent effect due to the Abel inversion. The path integrated absorptances were flat topped at their centers; thus the reduced profiles must exhibit a peak. The peak probably results from the wake formed from the initial boundary layers, or from the use of heating tapes wrapped about the pipes carrying test gas and hydrogen fluoride. Spectroscopically, the highest temperatures are indicated as being in the peak; the temperature measured by the thermocouple is taken to be that in the peak.

Mixing layer widths are plotted versus nondimensional mass flux difference in Fig. 22. The data is taken from Fig. 12 to 21 as well as from a few further experiments. In general, the results show increased mixing layer width for increased mass flux difference, and decreased mixing at increased Mach number level. The mixing layer widths are taken as the distance from the peak partial pressure to the point where the partial pressure is 2% of its peak value. The obtained widths are much larger than those predicted by mixing layer growth rate formulas, i.e. Eq. (17) or (18)

evaluated at Z = 0.59 in. Thus, it appears that free stream turbulence and the wake formed from the initial boundary layers dominate the mixing. Only at large values of nondimensional velocity difference do the results approach values predicted by Eq. (17) and (18). Furthermore, the mixing layer widths are fairly insensitive to gas type.

Since the selection of the "correct" mixing layer width is sensitive to the shape of the HF partial pressure profile in the vicinity of the inner and outer jet cores, the partial pressure half-radius, being more easily selected, was determined. The half-radius, defined as the point where P_{HF} is equal to one-half its core value, is plotted in Fig. 23 versus the mixing parameter of Eq. (18) with ρ_∞ set equal to the air jet density. The results are fairly successful in that a linear increase with mixing parameter is indicated. The half-radii of the hydrogen mixing layers are situated at greater radial distance than those for the nitrogen jets. Thus for similar mixing layer widths, the areal extent of mixed hydrogen and air is greater than that for mixing of nitrogen and air. For zero velocity difference the mixing layer half-radii appear to be centered at the radius of the inner jet injector tube—as intuitively expected. Half-radii for mixing layers of submerged N_2 and H_2 jets are also shown; the values appear to be consistent with those for mixing layers between coflowing jets.

In tests conducted with submerged subsonic air jets, hydrogen fluoride was centrally injected into the jet. Injector tube sizes of 1/4 in. o.d. and

3/16 in. o.d., with respective inside radii of 0.105 in. and 0.070 in., were employed. The profiles shown in Fig. 24 and 25 are nondimensionalized with their centerline values and injector tube inside radius. The air jet Mach number was 0.34. To reduce temperature dependence in the spectroscopic measurements, the J = 4 HF spectral line was selected. Profiles at several axial positions have been obtained. Based on a core length of four nozzle diameters, as given by Abramovich[8], the subsonic air jet at axial position Z = 3.03 in. should be almost free of a potential core. The very steep slope of the partial pressure profile at the centerline indeed indicates the lack of a core.

The ratio formed from the half-radius divided by the axial distance from the nozzle exit is shown below in Table 2.

Table 2. Partial Pressure Half Radius for Subsonic Jet Injected with Hydrogen Fluoride

Z in.	$r_{1/2}$ in.	$r_{1/2}/Z$
3.03	0.420	0.138
1.94	0.371	0.191
1.0	0.224	0.224
0.5	0.116	0.232

Thus, as the air jet approaches a fully developed condition and the hydrogen fluoride is completely mixed with the moving air, the half-radius appears to approach that given by Abramovich[8], i .e. $(r_{1/2})/Z = 0.097$, for velocity. Furthermore, since the hydrogen fluoride has a low velocity due to its high molecular weight, 50, and restricted cylinder pressure, 25 psia, suction by the air jet is necessary for its successful injection. One probably cannot treat this case as a classical mixing between coaxial hydrogen fluoride and air jets; rather, the flow situation is similar to that encountered during smoke injection into a moving stream.

V. SUPERSONIC COMBUSTION

Supersonic combustion is obtained using the high pressure three phase arc heater with plug nozzle. The arc heated air forms the outer jet, while the centrally injected cold hydrogen fuel with hydrogen fluoride tracer forms the inner jet of the free, coaxial, turbulently mixing jet system. Temperatures sufficient for auto-ignition of hydrogen and oxygen at expanded air Mach numbers of 2.0 to 2.5 have been obtained by operating the arc chamber at about 2000^{o}K. Schlieren photographs of reacting and nonreacting jets are shown in Fig. 26 and 27, respectively. A vertical knife-edge, parallel to the jet system centerline, was used to show density gradients in the cross-stream direction.

For the reacting case the hydrogen flow rate was 0.002 lbm/sec while that of the air was 0.115 lbm/sec—slightly fuel lean. The arc chamber pressure was 195 psia and its temperature was 1800^{o}K. The air jet had a Mach number of 2.4, and appears to constrict the upper jet to sonic conditions. The comparison nonreacting case used nitrogen, at 0.007 lbm/sec, substituted for hydrogen. While the nondimensional mass flux difference between the initial streams is greater in the hydrogen case—indicating increased mixing—the amplified spreading rate of the composite submerged jet is felt to be mainly due to combustion and the effect of combustion on density and turbulent fluctuations. Based on the initial overall

diameter of the jet system at the nozzle exit, the reacting jet begins to spread more rapidly than the nonreacting jet at a distance of slightly more than two diameters downstream. This is interpreted as the start of significant combustion, and the corresponding time delay, for an average jet velocity of 4000 ft/sec, is 3×10^{-5} sec. (Until more experiments are performed, especially with hydrogen fluoride, we refrain from calling this time the ignition delay.) The density difference between inner and outer jets is detectable at greater distances in the nonreacting case than in the reacting case; this also indicates increased cross-stream mixing in the reacting case.

A large extent of the reacting jet—mainly the region encompassed by the photograph of Fig. 26—appeared very luminous. Also, a thermocouple located in the exhaust stack approximately 7 ft above the nozzle exit detected a temperature of 335°F for the reacting jet, and 135°F for the nonreacting jet. Furthermore, the acoustic noise generated by the jet system was observed to be much louder in the combustion case.

Preliminary spectroscopic measurements using hydrogen fluoride have been obtained for the above inner jet flow conditions but with slightly different hot air conditions, i.e. chamber temperature of 2000°K and pressure of 115 psia, flow rate of 0.065 lbm/sec and expanded Mach number of 2.0. A trace of spectral output showing the J = 1 HF line at cold

conditions, and a subsequent radial scan of emission at combustion conditions is presented in Fig. 28. The optics were centered 2.38 in., i.e. 3 1/2 diameters, downstream from the nozzle exit; the black body temperature of the lamp at the wavelength corresponding to the J = 1 HF spectral line was 1150°K. The trace indicates the following: (1) For the nonreacting case with arc heated air and nitrogen center jet—similar to Fig. 27—absorption of the light source radiation by the hydrogen fluoride still existed. However, its value was much reduced from the cold conditions, i.e. 6% with arc heater at operating temperature versus 30% cold, thus indicating some emission from the hot gases. An average temperature can be inferred by assuming that the jet is isothermal; its temperature would then be slightly below the black body source temperature of 1150°K. (2) With hydrogen replacing nitrogen in the center jet, the resulting combustion caused a net emission of energy. The jet system was radially scanned in the vicinity of its centerline over a distance of 0.35 in. Throughout, there was a net emission of energy; the maximum value was 15% greater than the light source background radiation. By comparison with the source temperature and the nonreacting spectral output the inferred temperature—greater than 1150°K for an assumed isothermal jet—indicates the occurrence of combustion.

Because the part of the HF spectrum examined is known to be isolated from regions of H_2O and CO_2 radiation, and since H_2, O_2, and N_2 are inactive, the measured emission is assumed due to HF. By comparing inferred temperatures with schlieren photographs showing shock waves, a significant region of combustion was observed to occur in the region where the flow was still predominantly supersonic. No evidence of combustion inhibition by the hydrogen fluoride was observed, that is, no change in the size or luminosity of the reacting jet was observed with and without hydrogen fluoride present. If reaction of HF with any species present in the reacting gases occurred—for instance HF + H_2O⟶hydrofluoride acid—it was insufficient to eliminate the spectrally active HF.

VI. CONCLUSIONS

This study was undertaken to develop tracer molecule diagnostics using hydrogen fluoride with application to turbulently mixing and reacting flows. Mixing in cold, radiatively absorbing jets has been investigated; the tracer technique appears to be very useful when the vapor state of the hydrogen fluoride is chemically frozen. Hydrogen fluoride concentration profiles can then be equated to those of the fluid which has been tagged with tracer. By proper selection of the hydrogen fluoride spectral line, temperature, and flow rate precise concentration profiles and mixing rates are determinable. The technique is an important diagnostic aid in compressible flows where a physical probe would adversely affect the turbulent structure.

For radiatively absorbing jets the following suggestion is made: best results would be obtained with hydrogen fluoride vapor completely monomer, and therefore it may be desirable to heat the hydrogen fluoride to temperatures of $350^{o}K$ and premix it with the desired test gas for a sufficient time in a special cylinder. Also, cold supersonic jets may be investigated since the inclusion of test gas effectively causes the hydrogen fluoride to supersaturate; thus condensation is eliminated. For hot reacting flows hydrogen fluoride condensation and polymerization should not be a problem. Furthermore, as indicated by LaPointe[3], it is

possible to determine temperature in radiatively absorbing flows by ratioing the spectral output using two spectral lines.

Supersonic combustion in a submerged jet system has been obtained for the hydrogen-oxygen reaction. The combustion caused a marked increase in the jet spreading rate when compared to a nonreacting similar jet system using inert nitrogen substituted for hydrogen. Preliminary temperature determinations using hydrogen fluoride tracer in reacting jets have been made: at the wavelength corresponding to the J = 1 HF spectral line, a net emission of radiation occurred. Further studies are planned to advance the hydrogen fluoride tracer molecule diagnostic technique so that temperature, global reaction times, and mixing rates can be precisely determined in turbulent combusting flows.

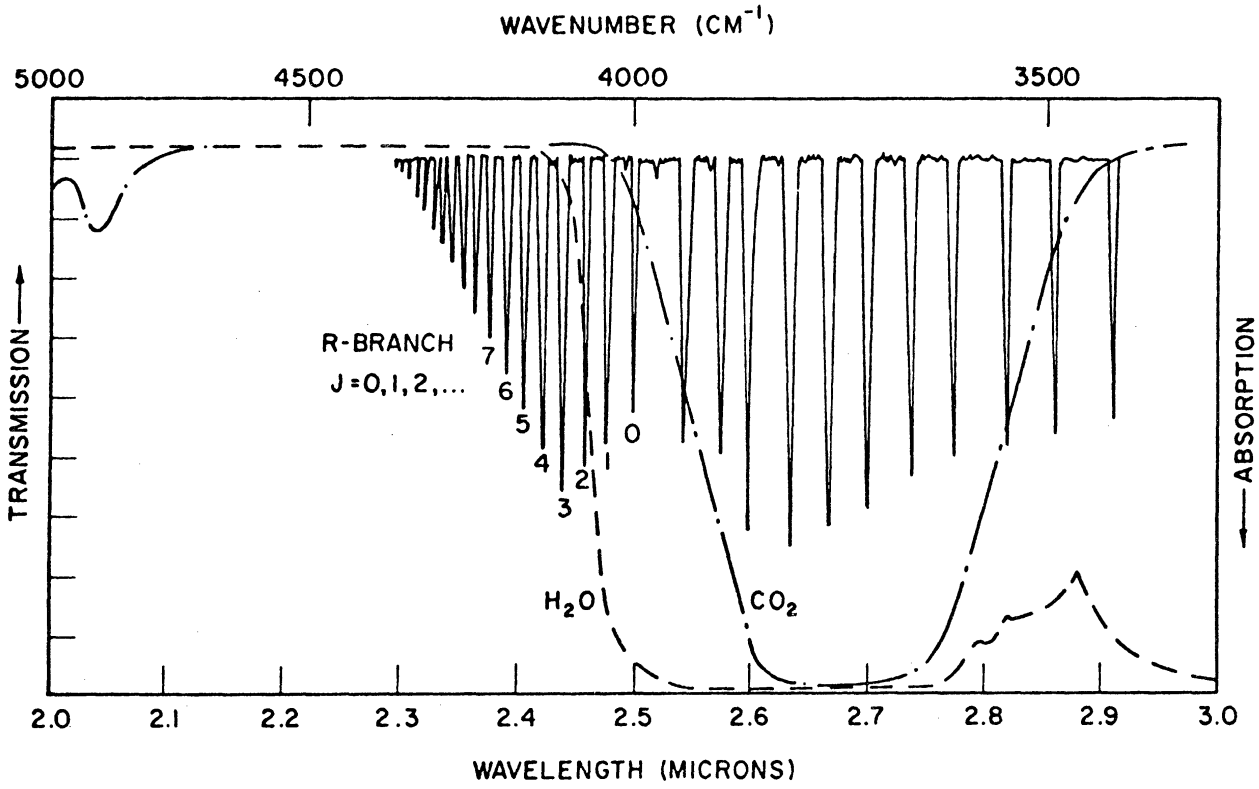

Figure 1. HF Fundamental Vibration-Rotation Absorption Band (R and P Branches). Spectral Location of Water and Carbon Dioxide Absorption Bands Indicated

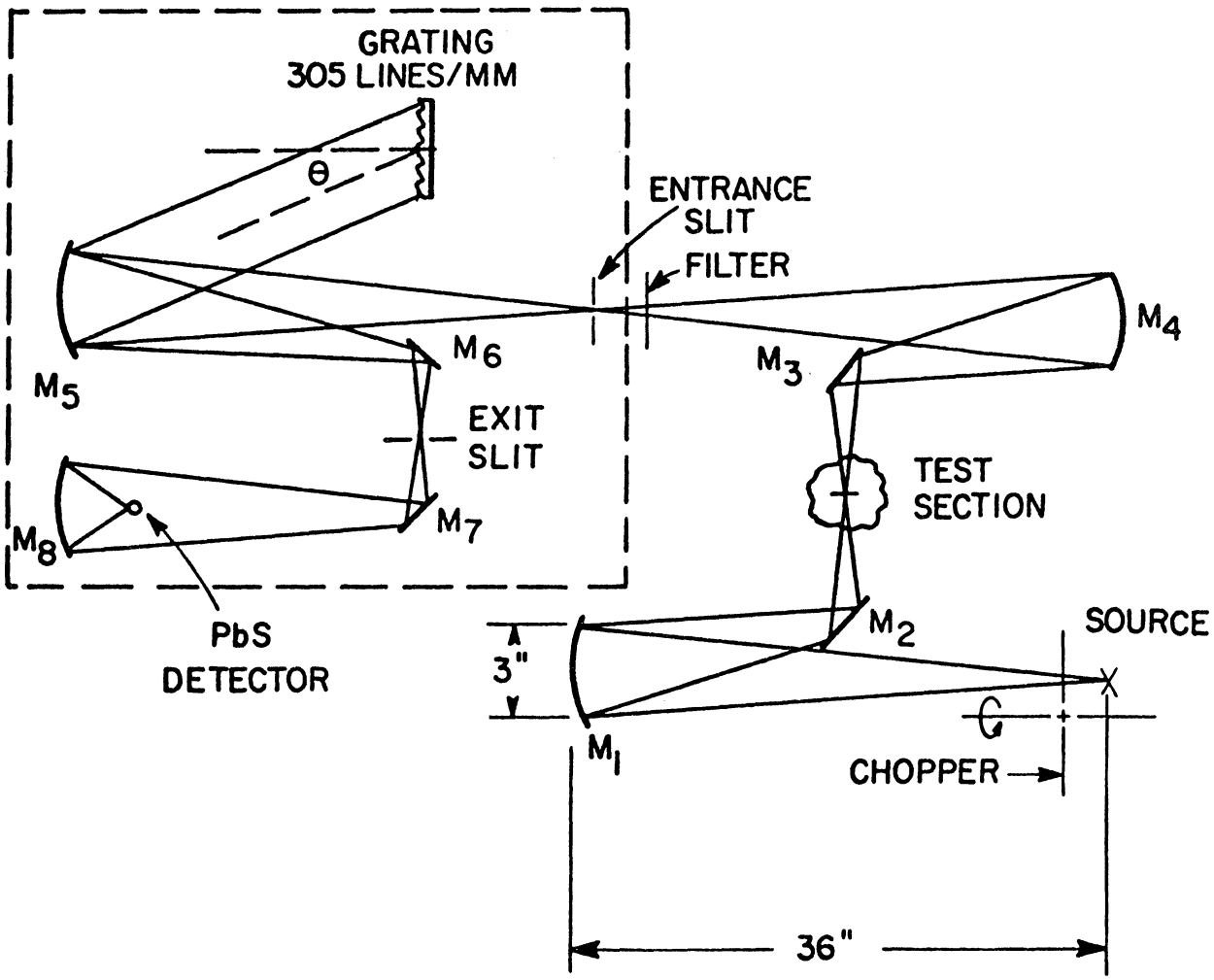

Figure 2. Monochromator and Entrance Optics Physical Schematic

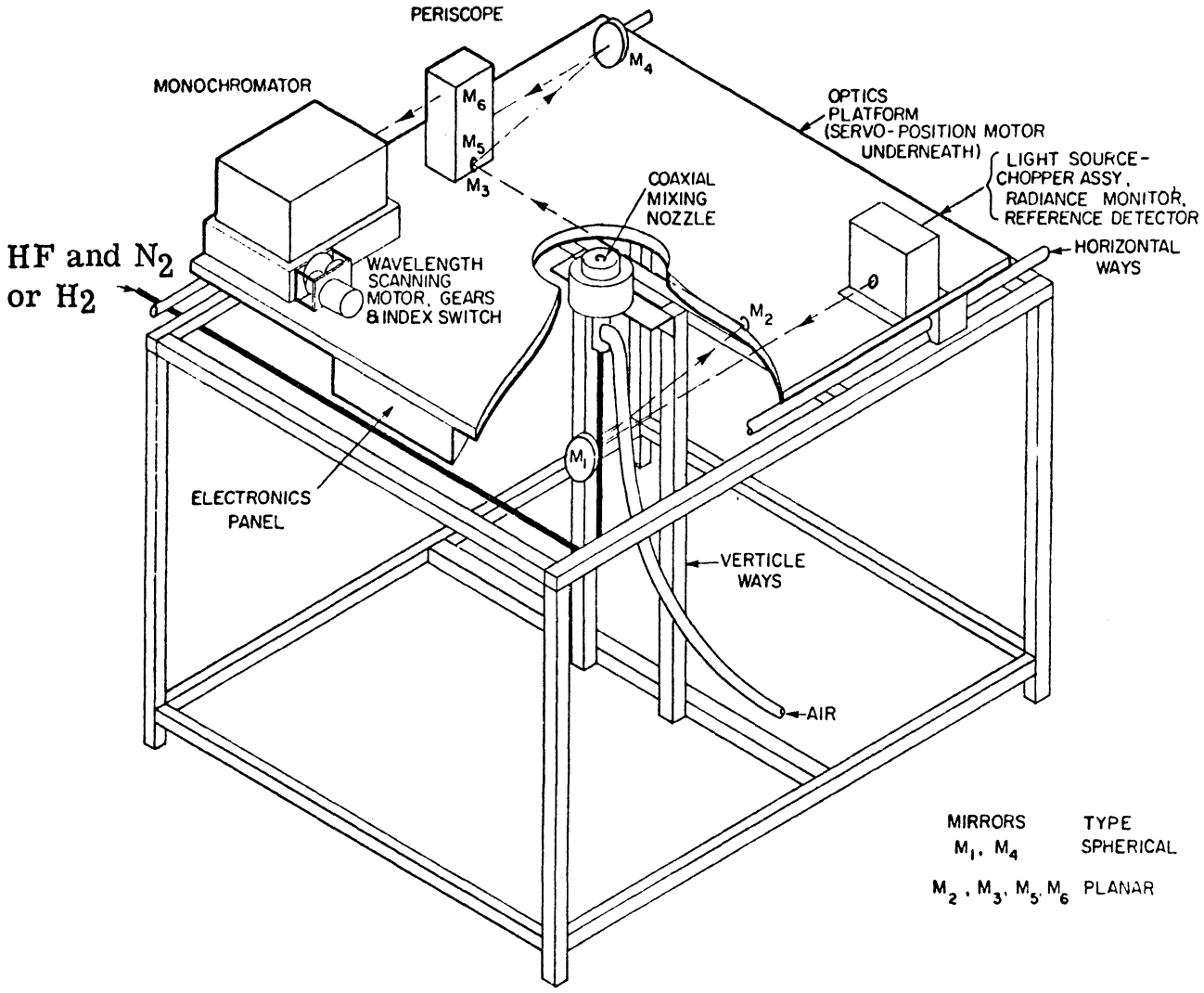

Figure 3. Jet Mixing Test Stand

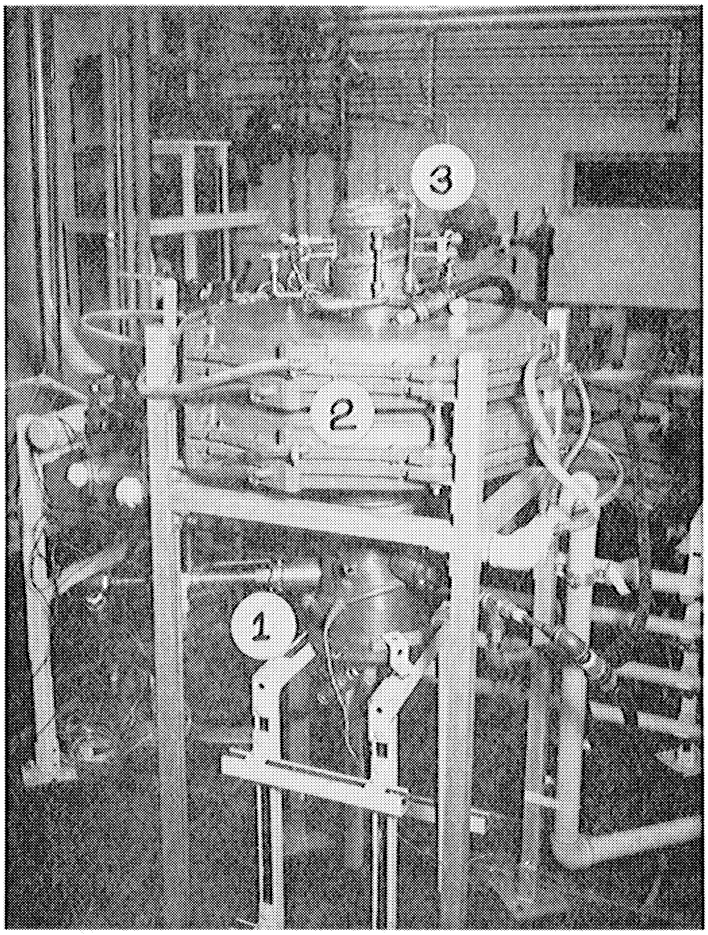

1. Arc Heater
2. Magnetic Coils
3. Plug Nozzle

Figure 4. Arc Heater with Magnetic Coils and Plug Nozzle.

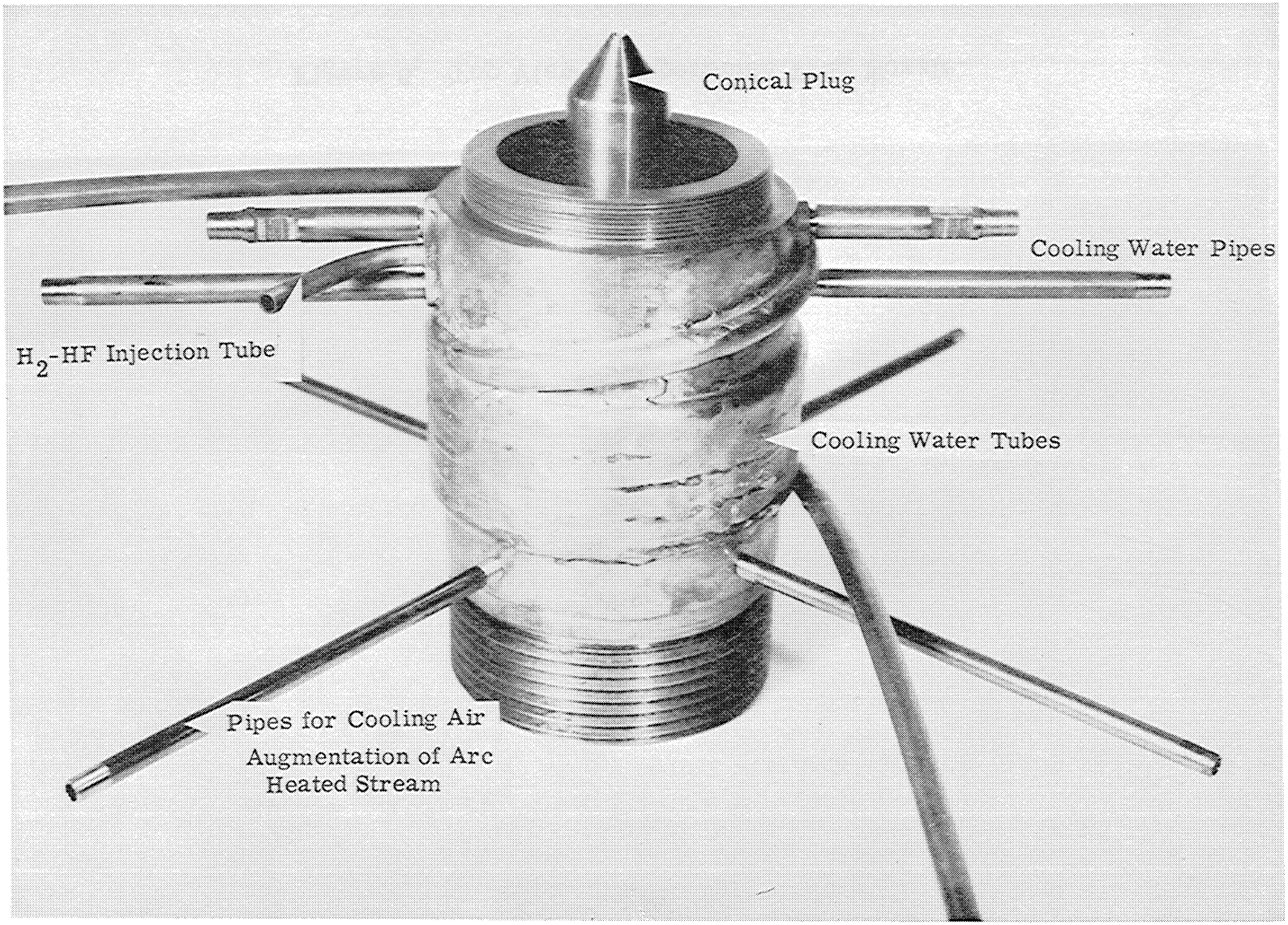

Figure 5. Plug Nozzle Bottom Section with Conical Plug.

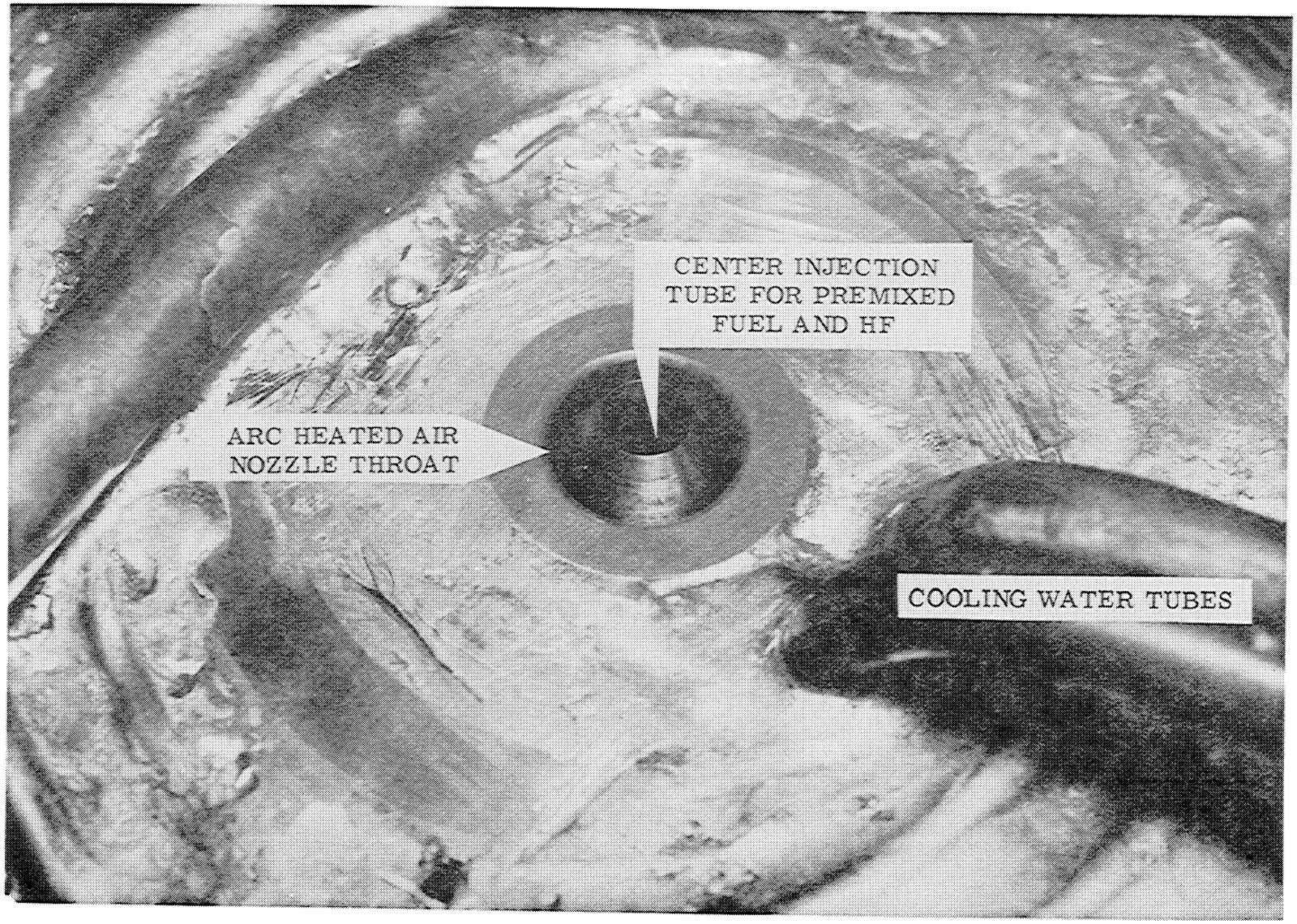

Figure 6. Top View of Supersonic Plug Nozzle.

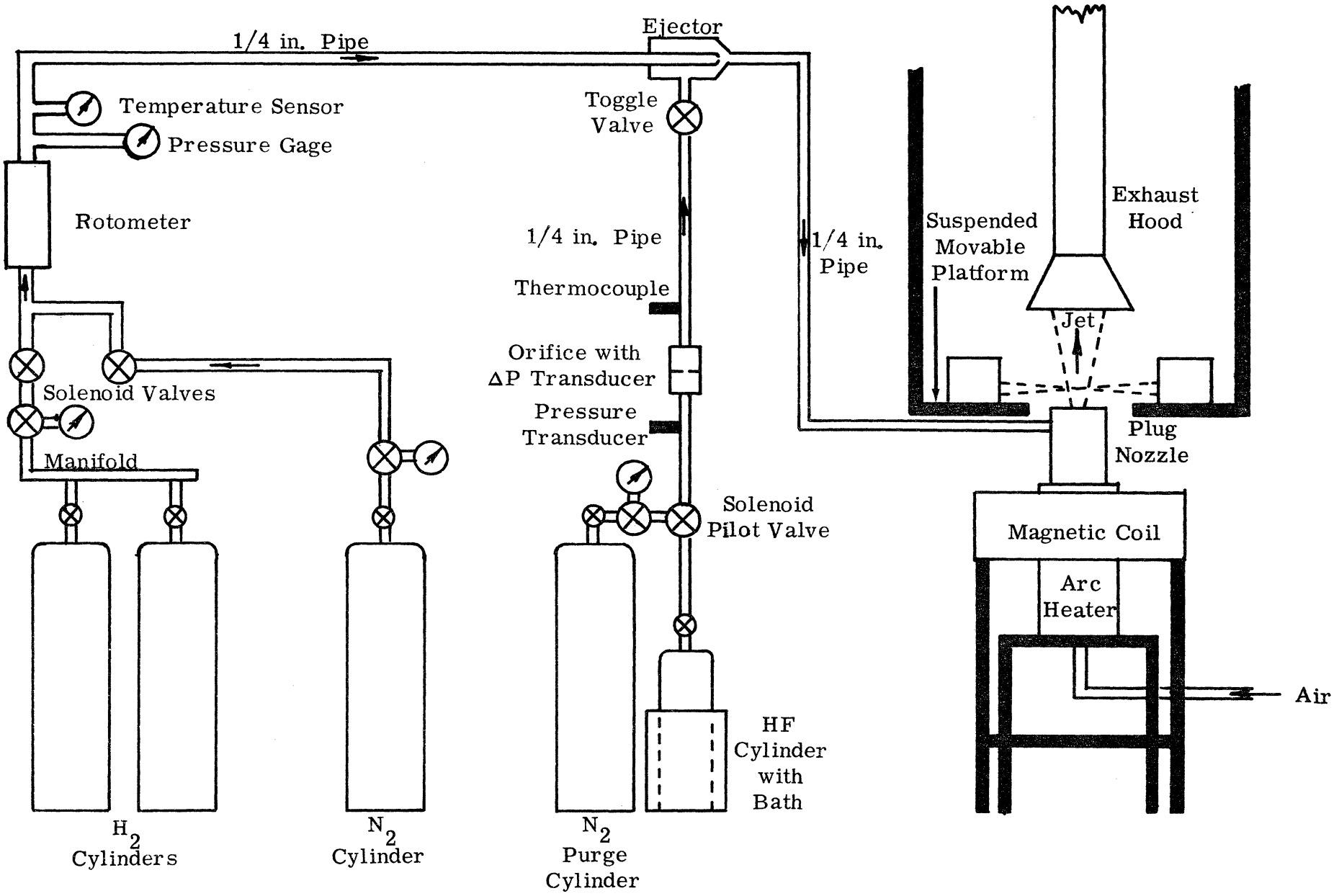

Figure 7. Schematic of Supersonic Combustion Experiment.

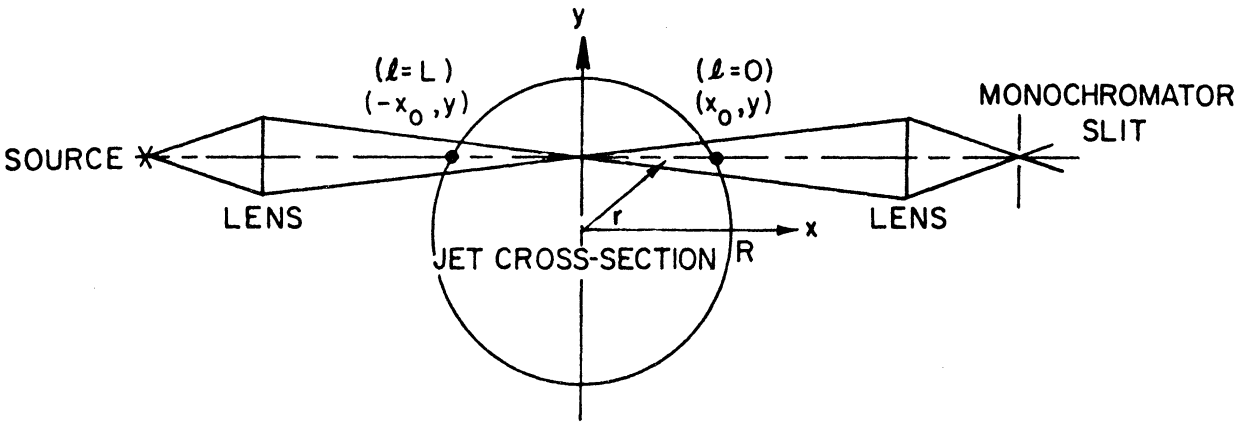

Figure 8. Spectroscopic Coordinate System

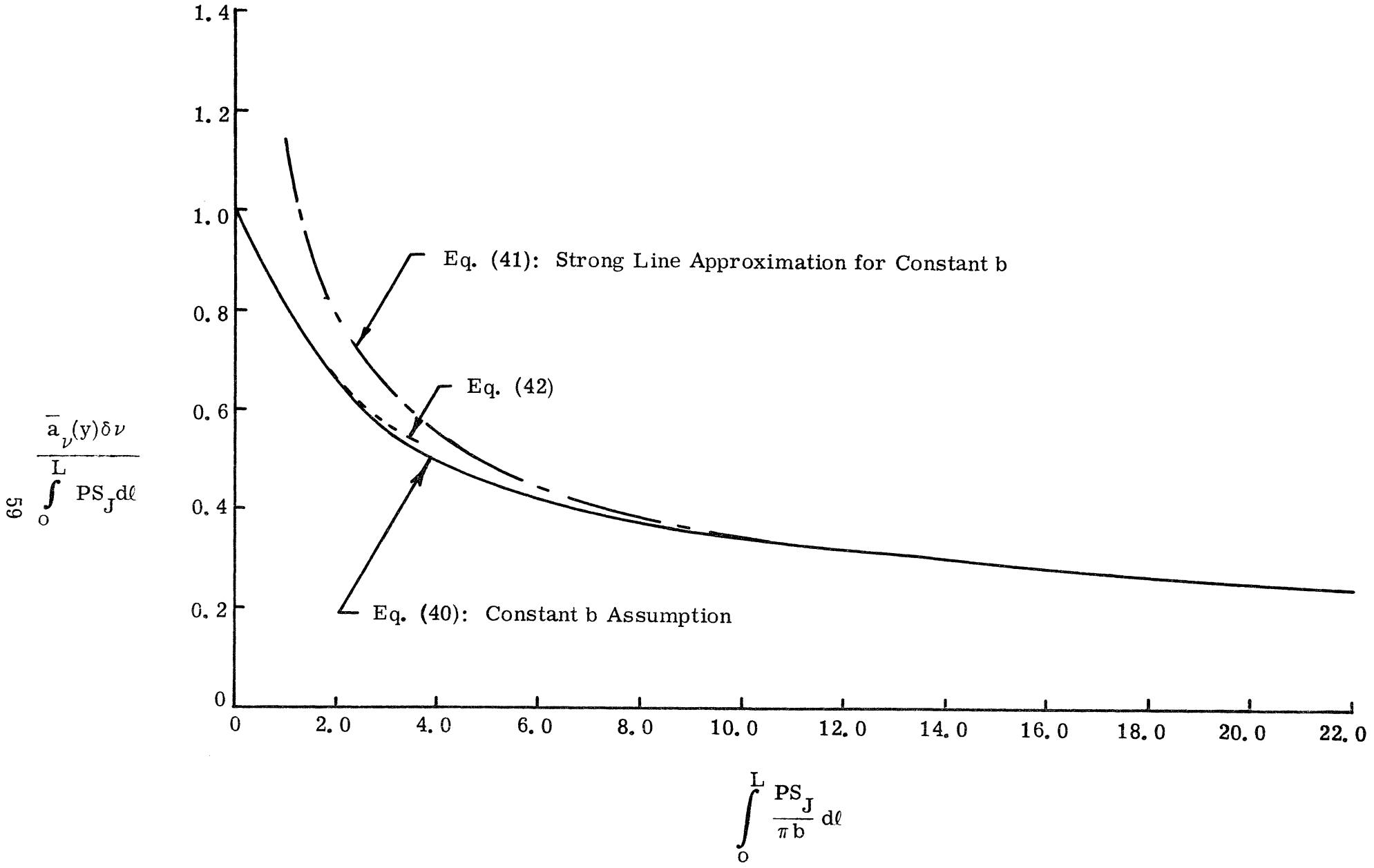

Figure 9. Measured Absorptance Related to $\int_0^L PS_J d\ell$ Assuming Constant Spectral Line Half-Width.

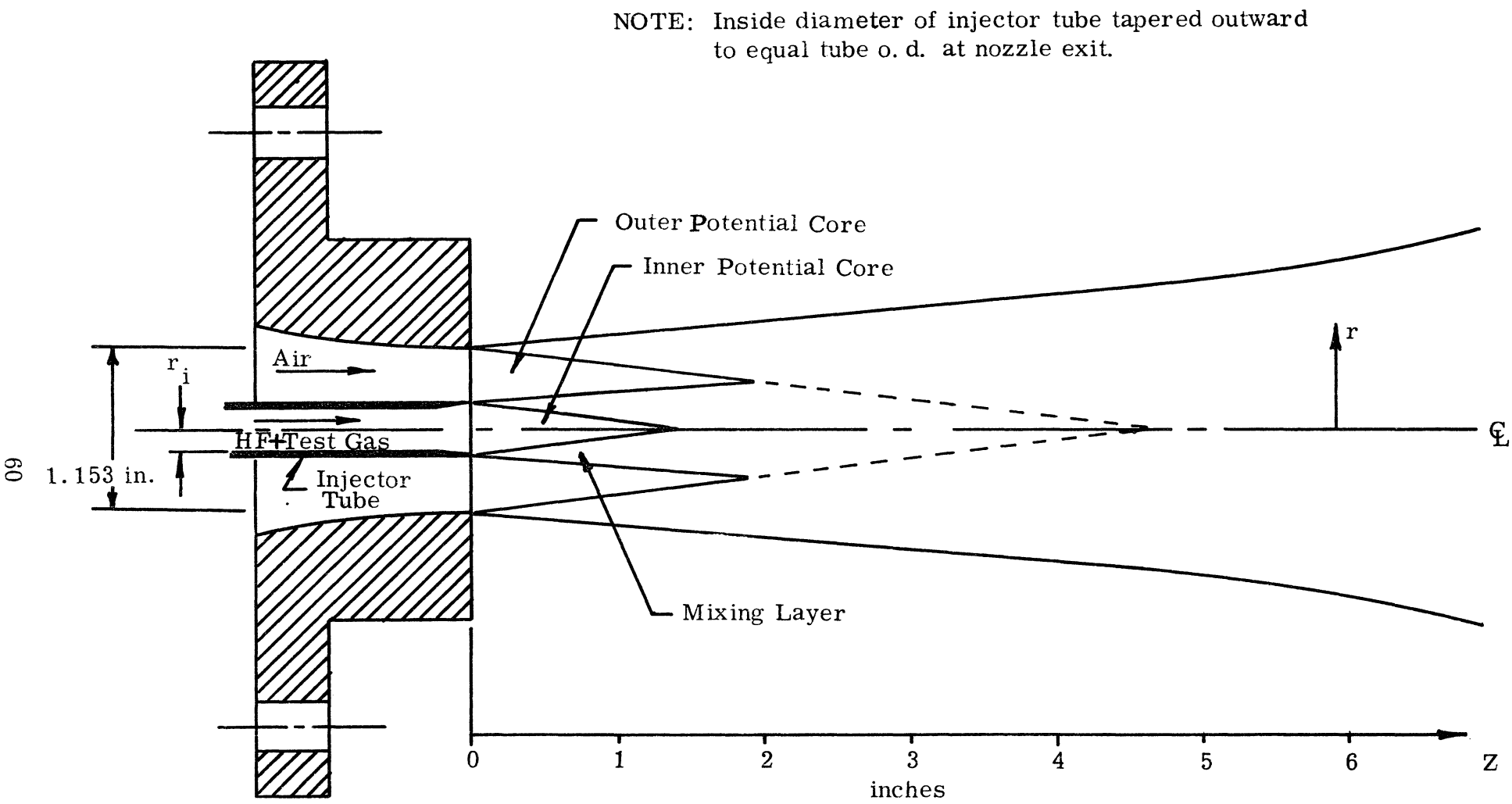

Figure 10. Coaxial Free Jet Mixing Configuration for Absorption Experiments.

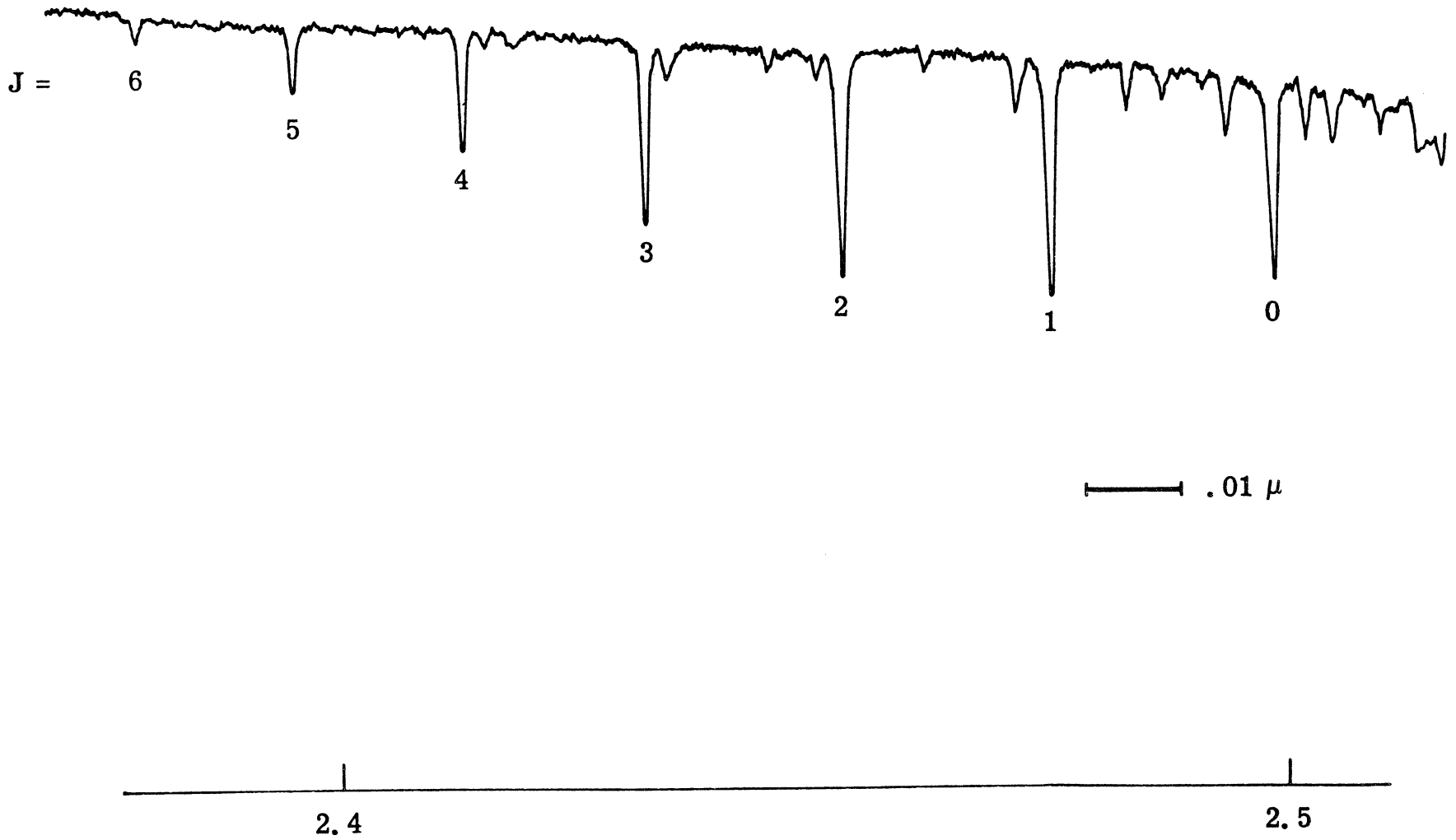

Figure 11. HF Absorption Spectrum Showing First Seven Lines of R-Branch

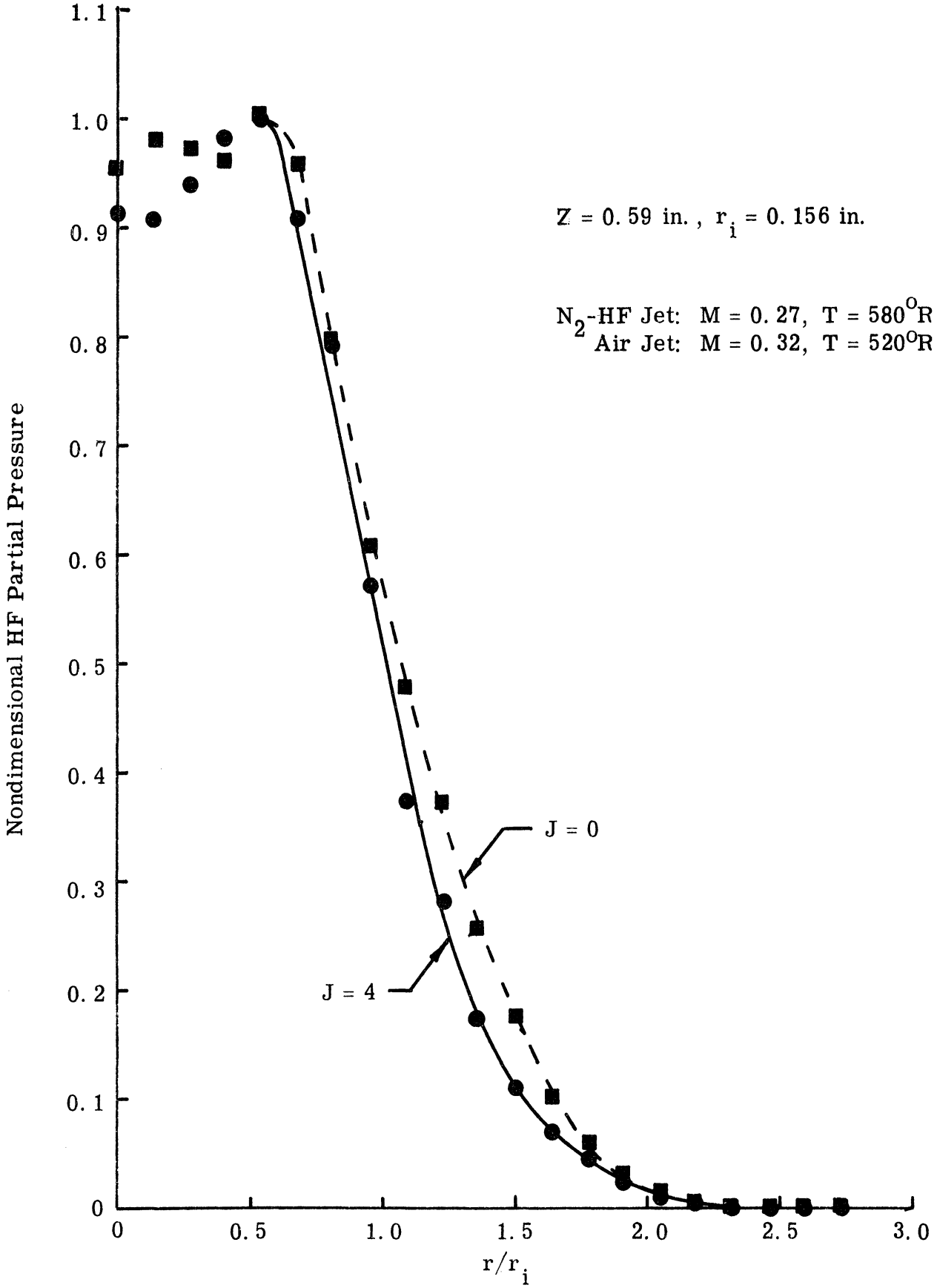

Figure 12. Coaxial Mixing Layer Between Inner N_2-HF Jet and Outer Air Jet.

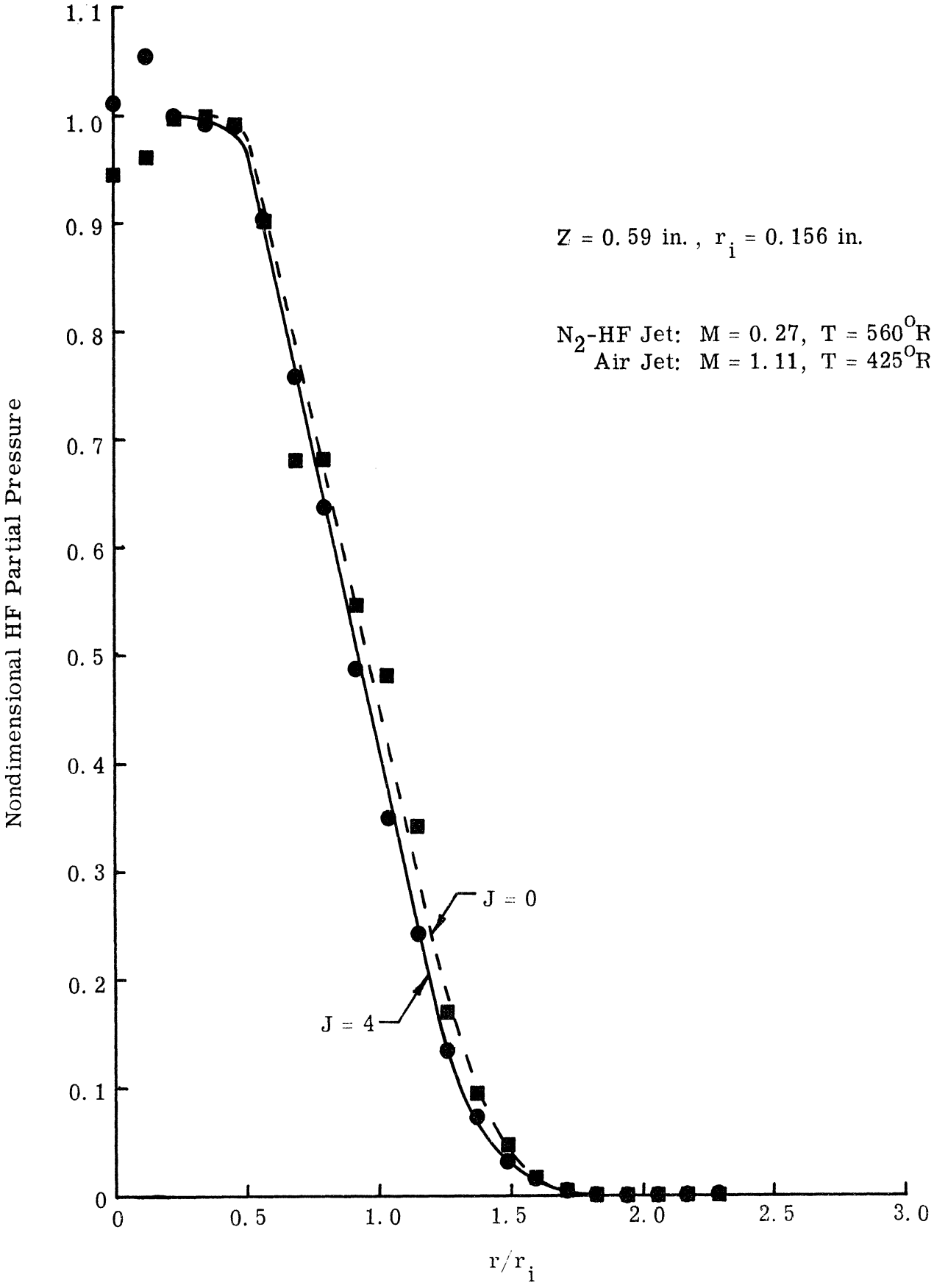

Figure 13. Coaxial Mixing Layer Between Inner N_2-HF Jet and Outer Air Jet.

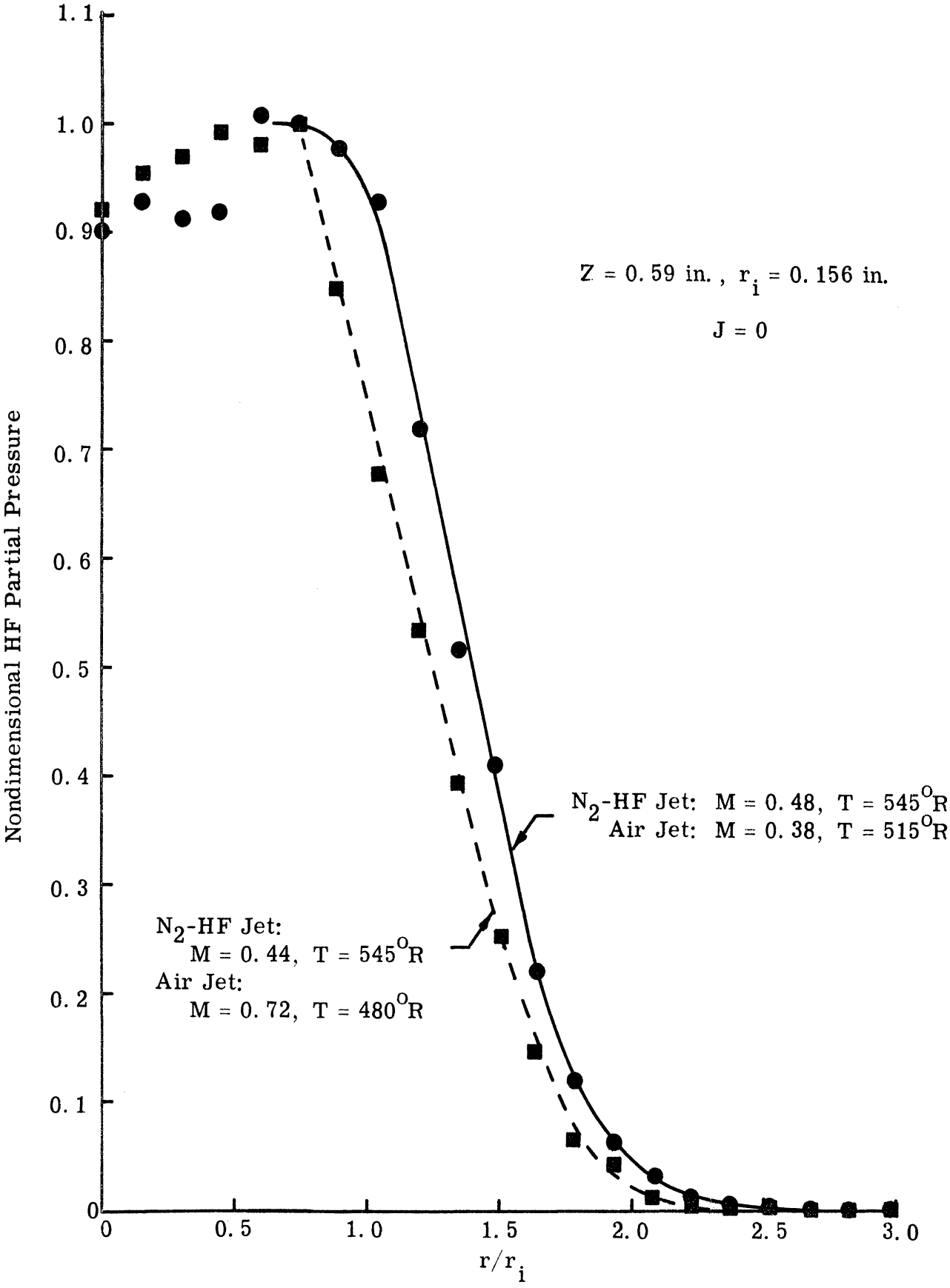

Figure 14. Coaxial Mixing Layer Between Inner N_2-HF Jet and Outer Air Jet.

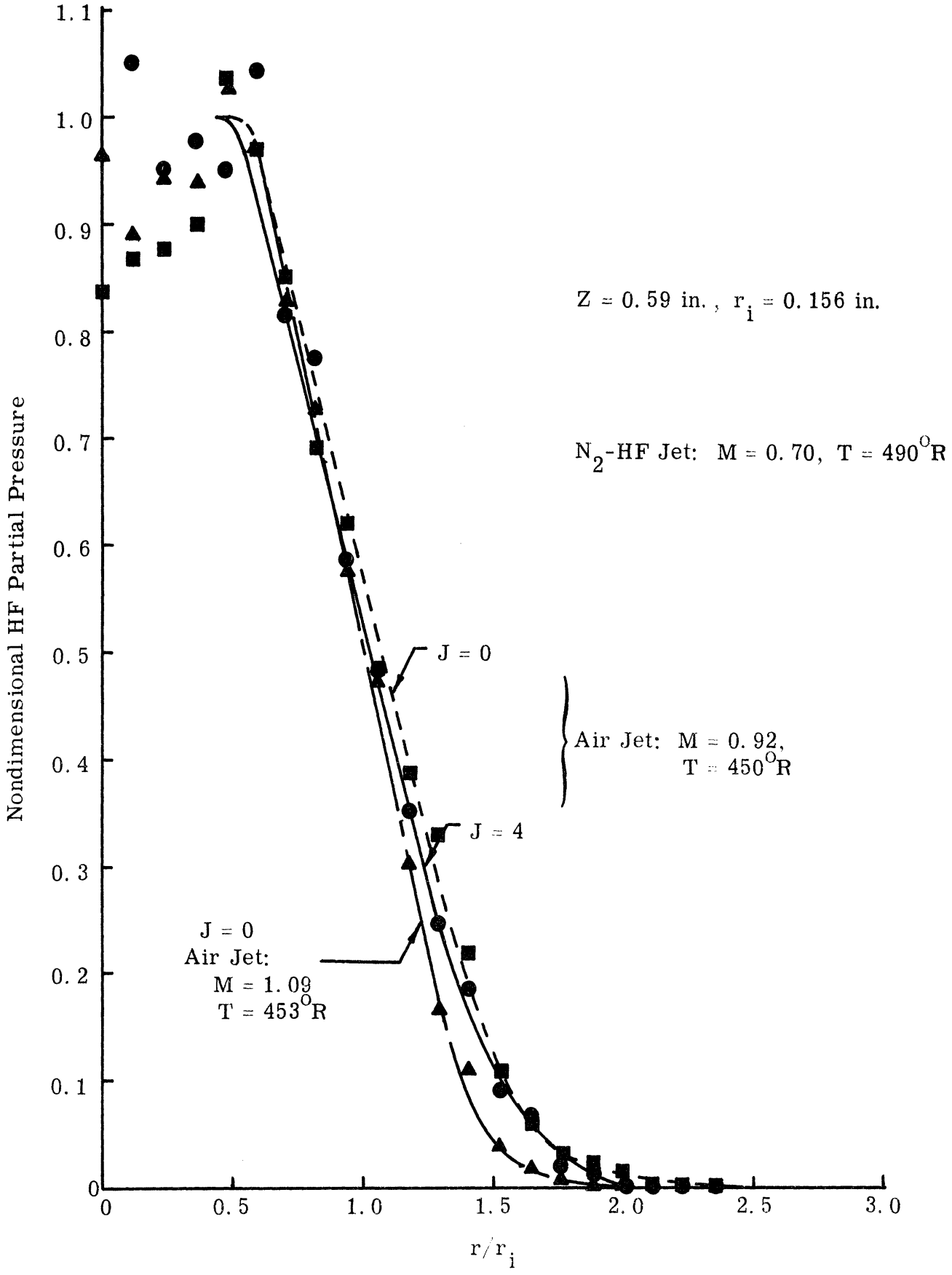

Figure 15. Coaxial Mixing Layer Between Inner N_2-HF Jet and Outer Air Jet.

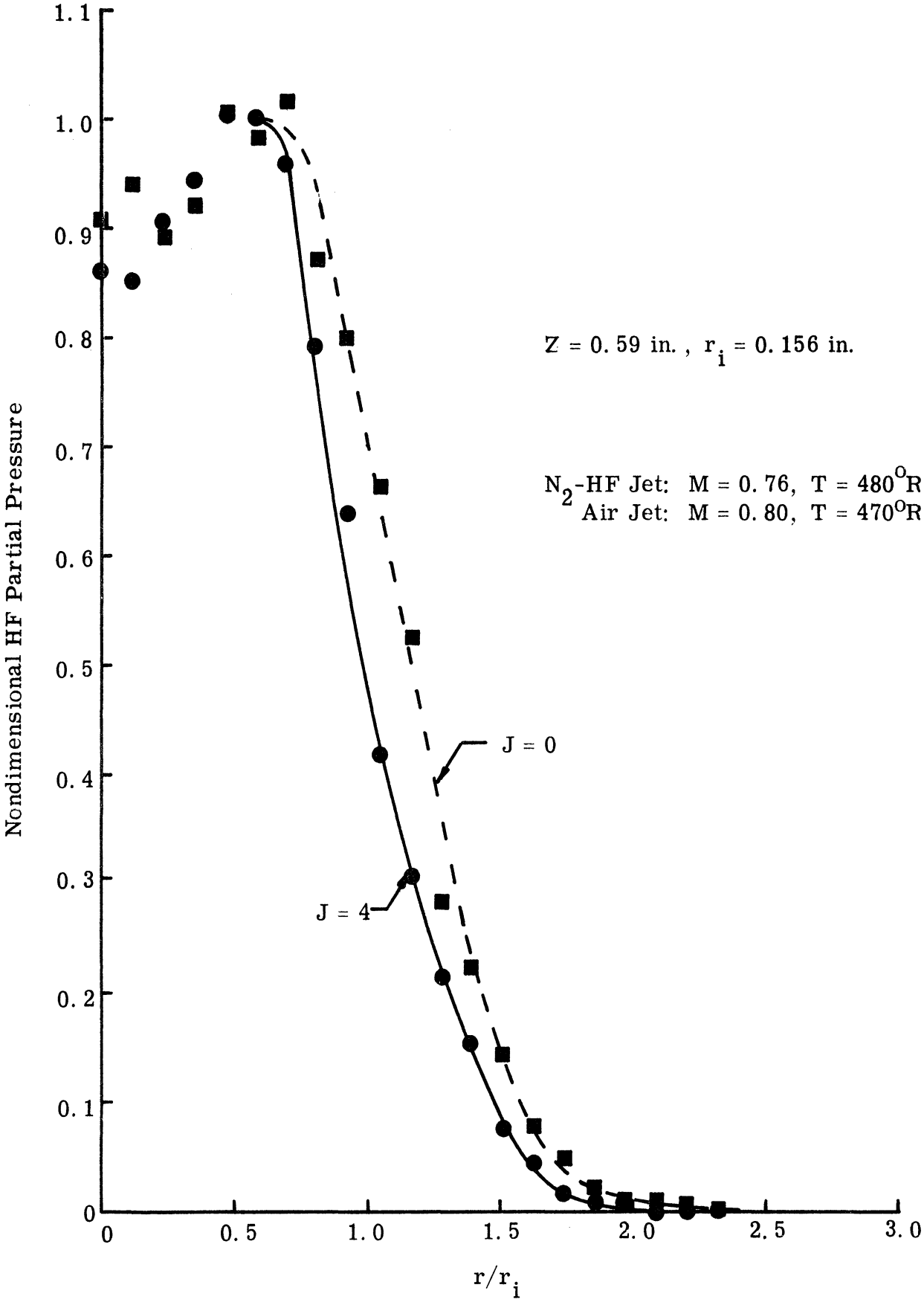

Figure 16. Coaxial Mixing Layer Between Inner N_2-HF Jet and Outer Air Jet.

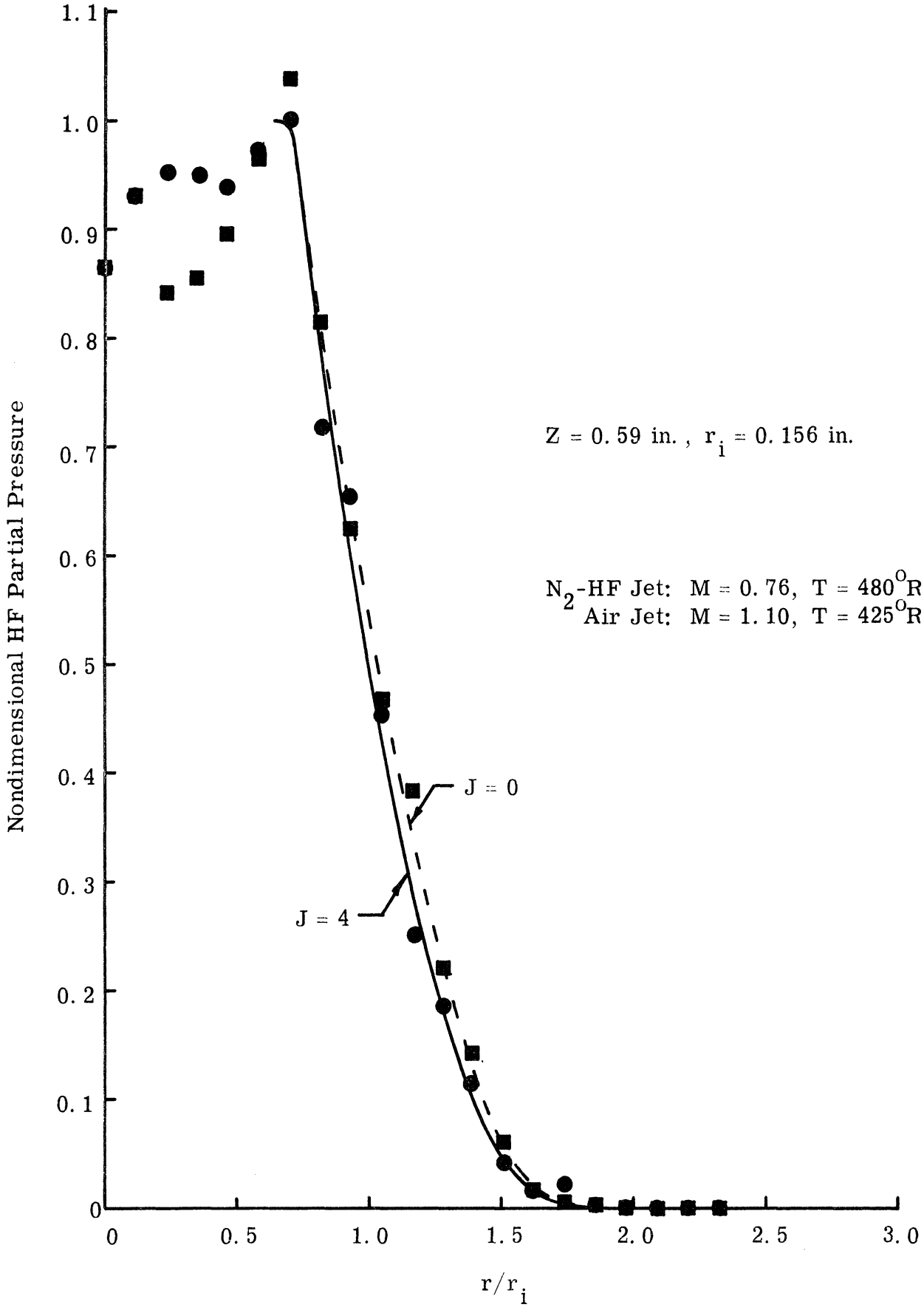

Figure 17. Coaxial Mixing Layer Between Inner N_2-HF Jet and Outer Air Jet.

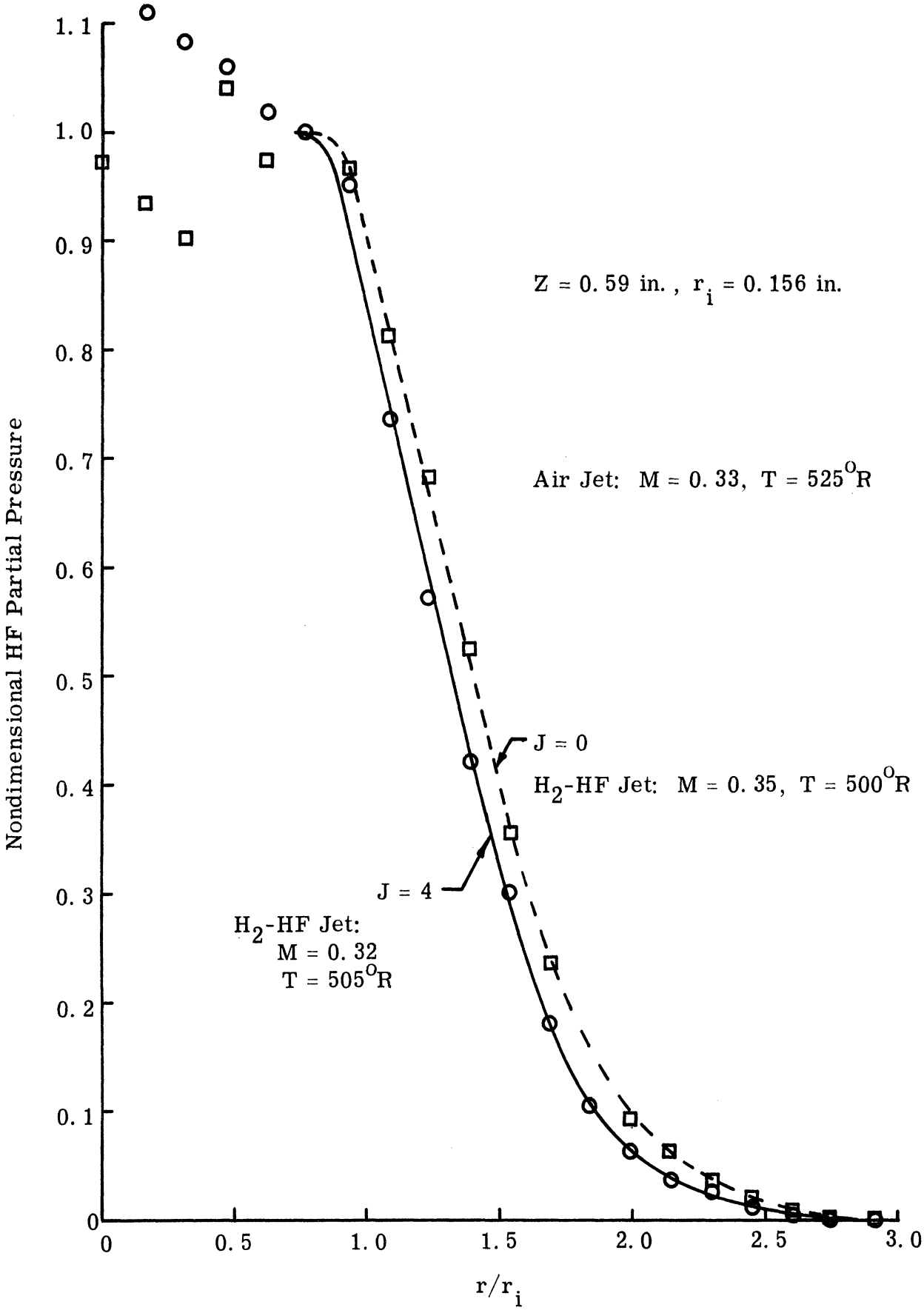

Figure 18. Coaxial Mixing Layer Between Inner H_2-HF Jet and Outer Air Jet.

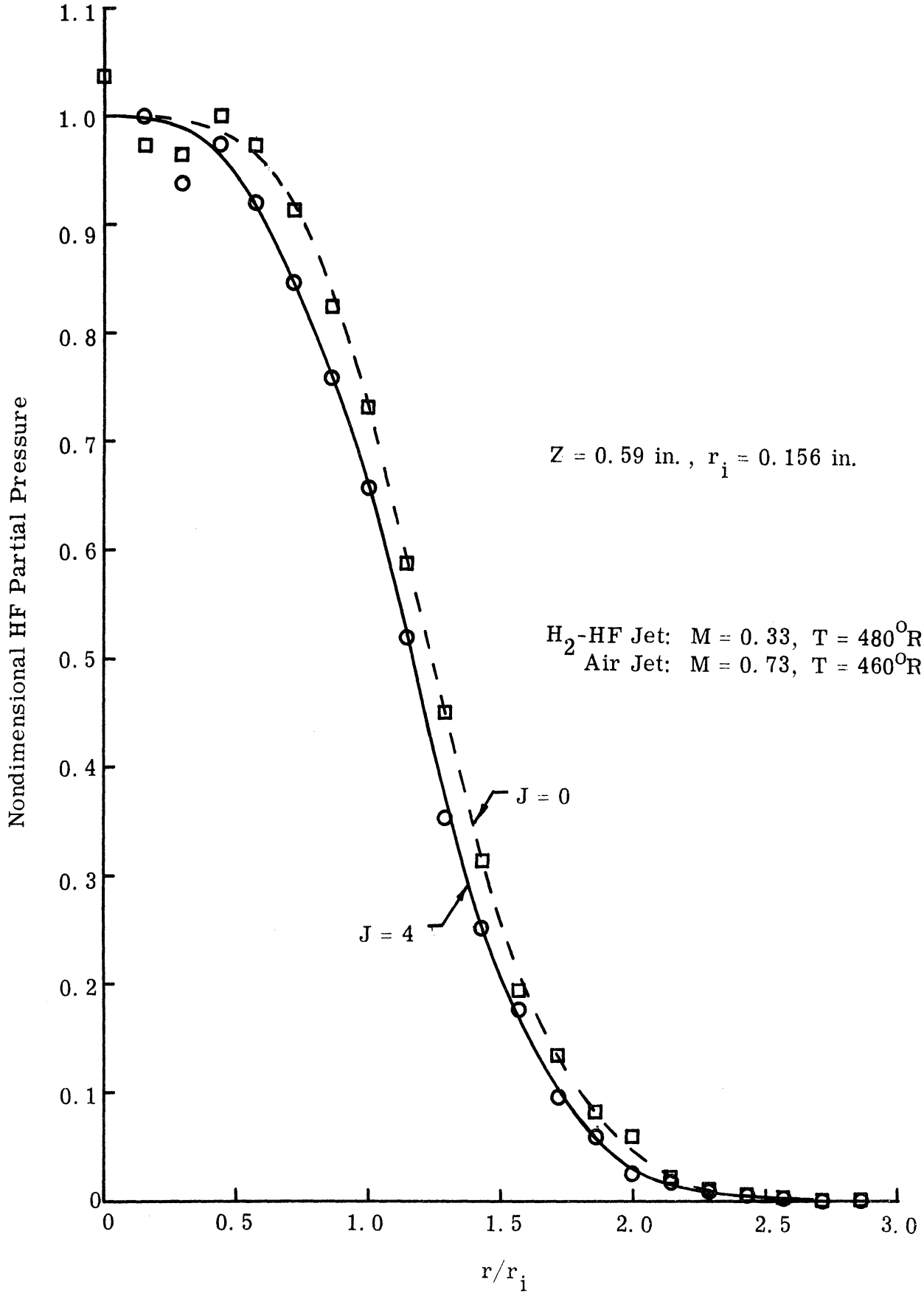

Figure 19. Coaxial Mixing Layer Between Inner H_2-HF Jet and Outer Air Jet.

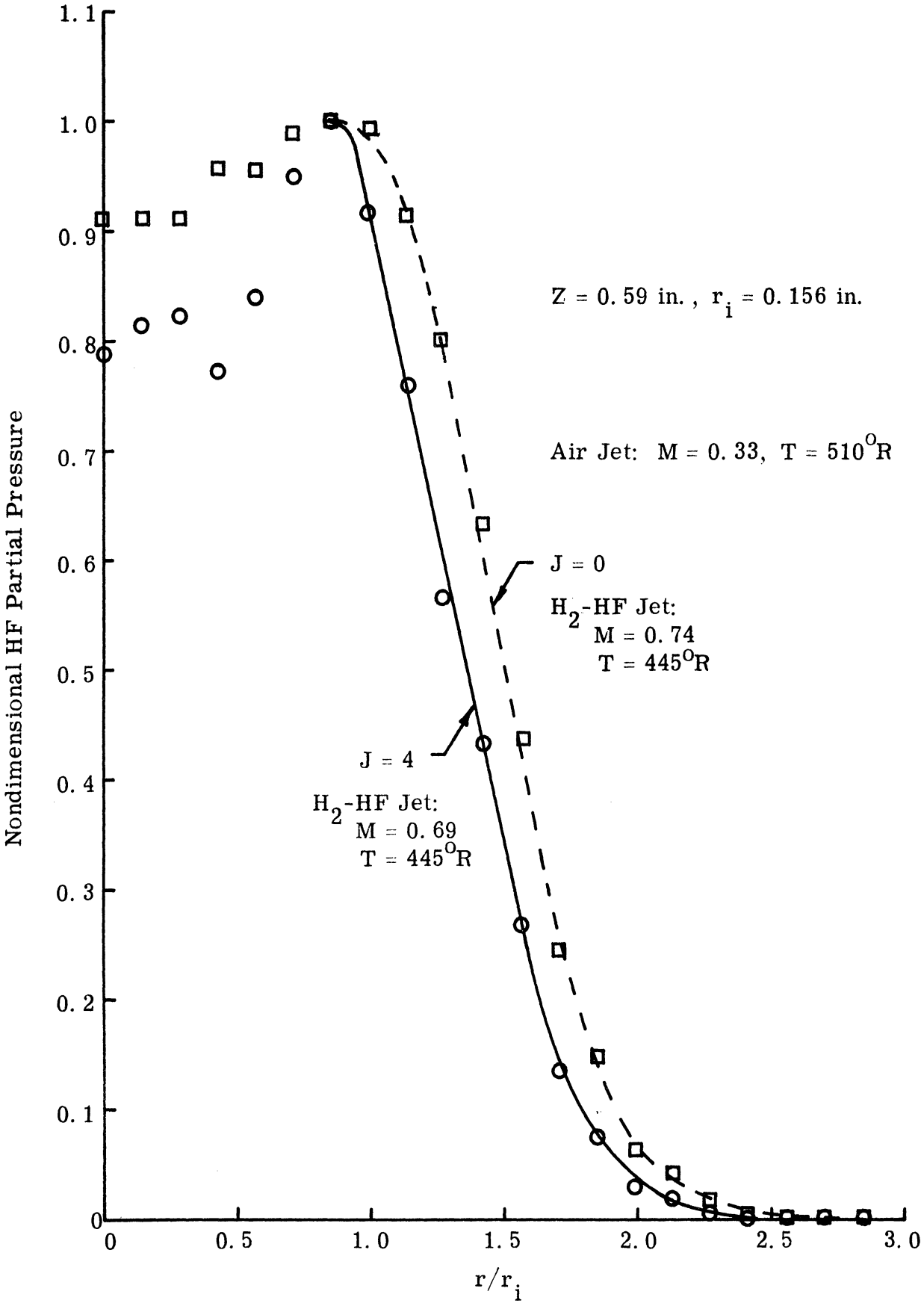

Figure 20. Coaxial Mixing Layer Between Inner H_2-HF Jet and Outer Air Jet.

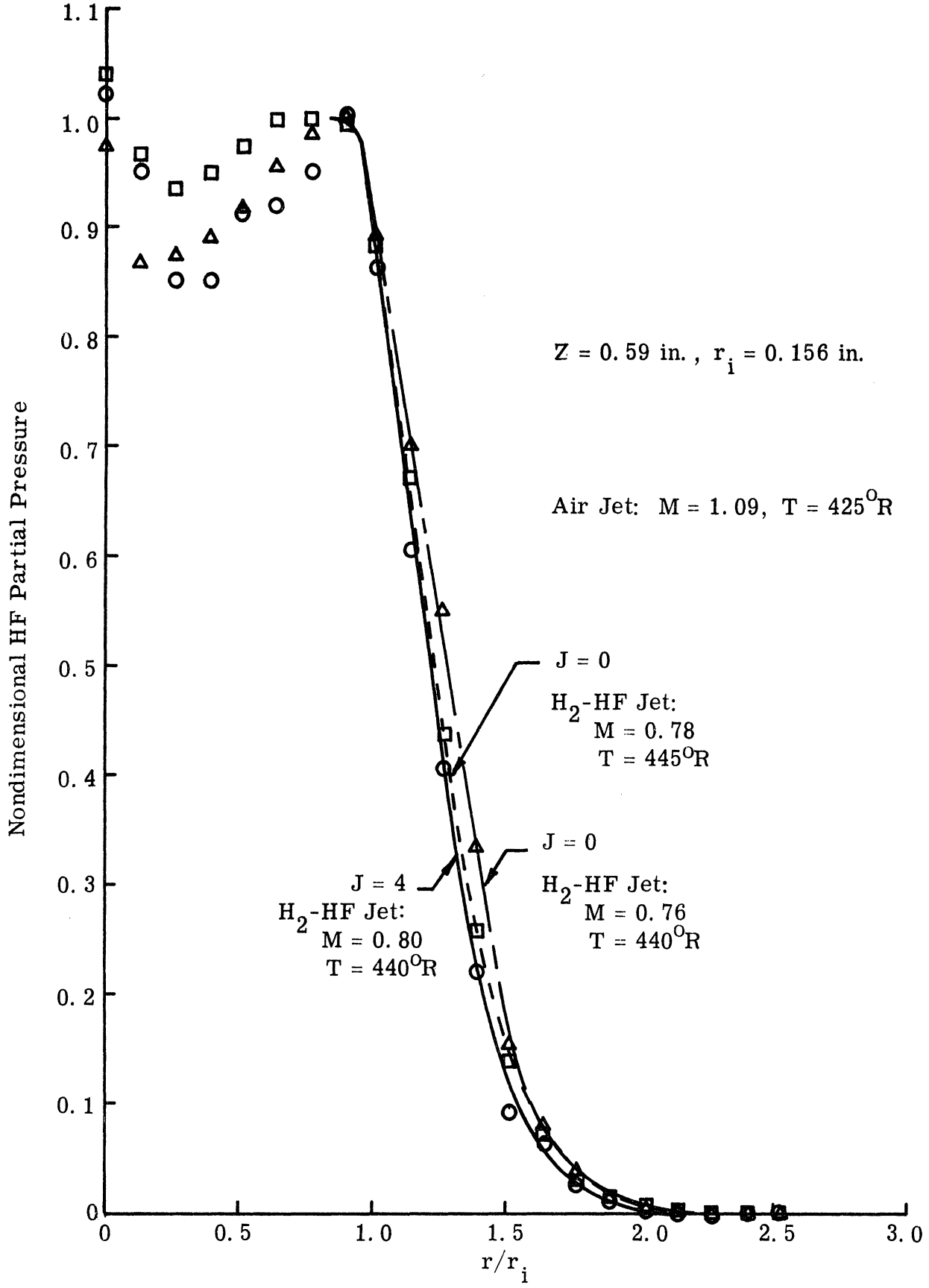

Figure 21. Coaxial Mixing Layer Between Inner H_2-HF Jet and Outer Air Jet.

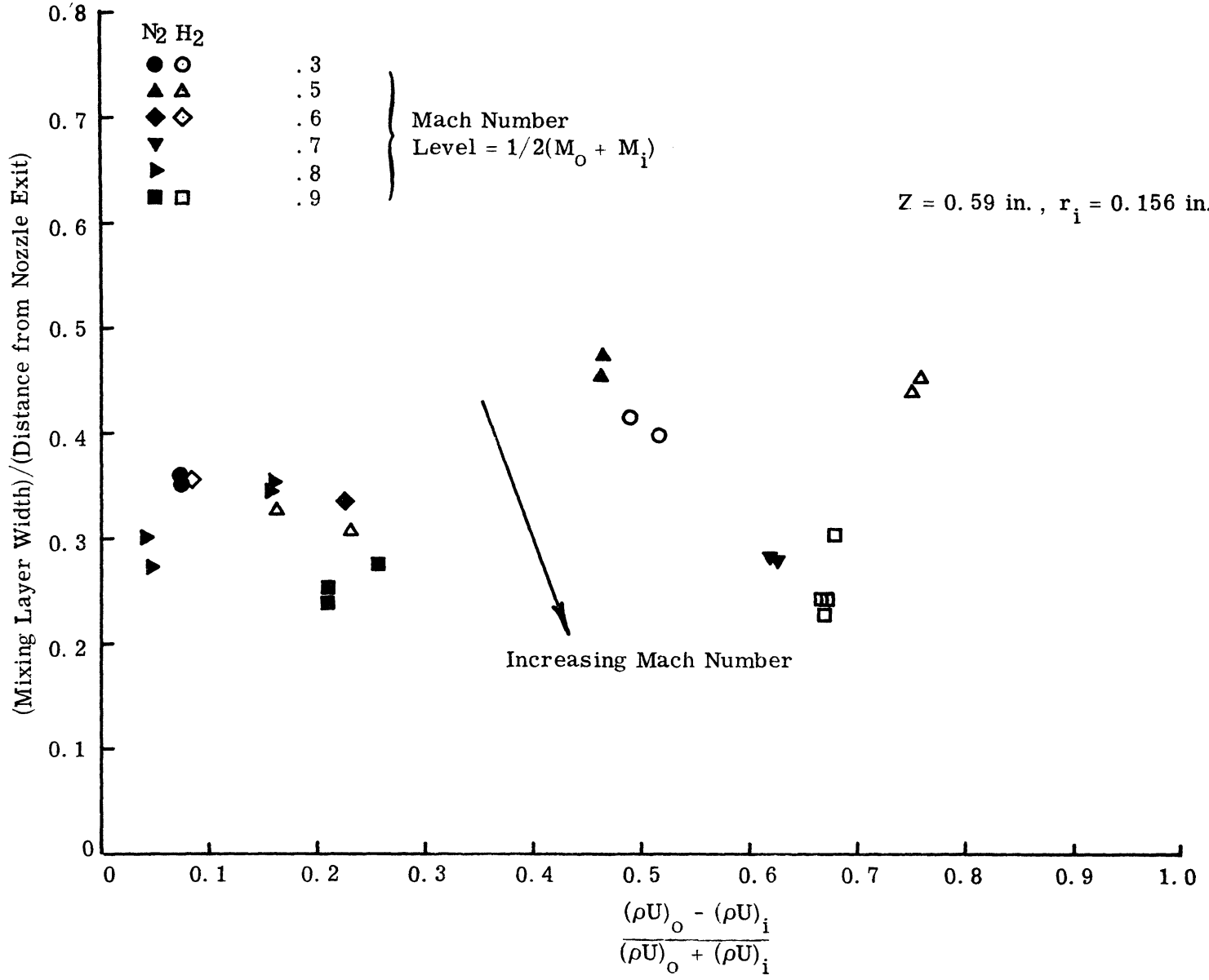

Figure 22. Mixing Layer Widths Between Inner Jets of Nitrogen and Hydrogen Mixing with an Outer Air Jet.

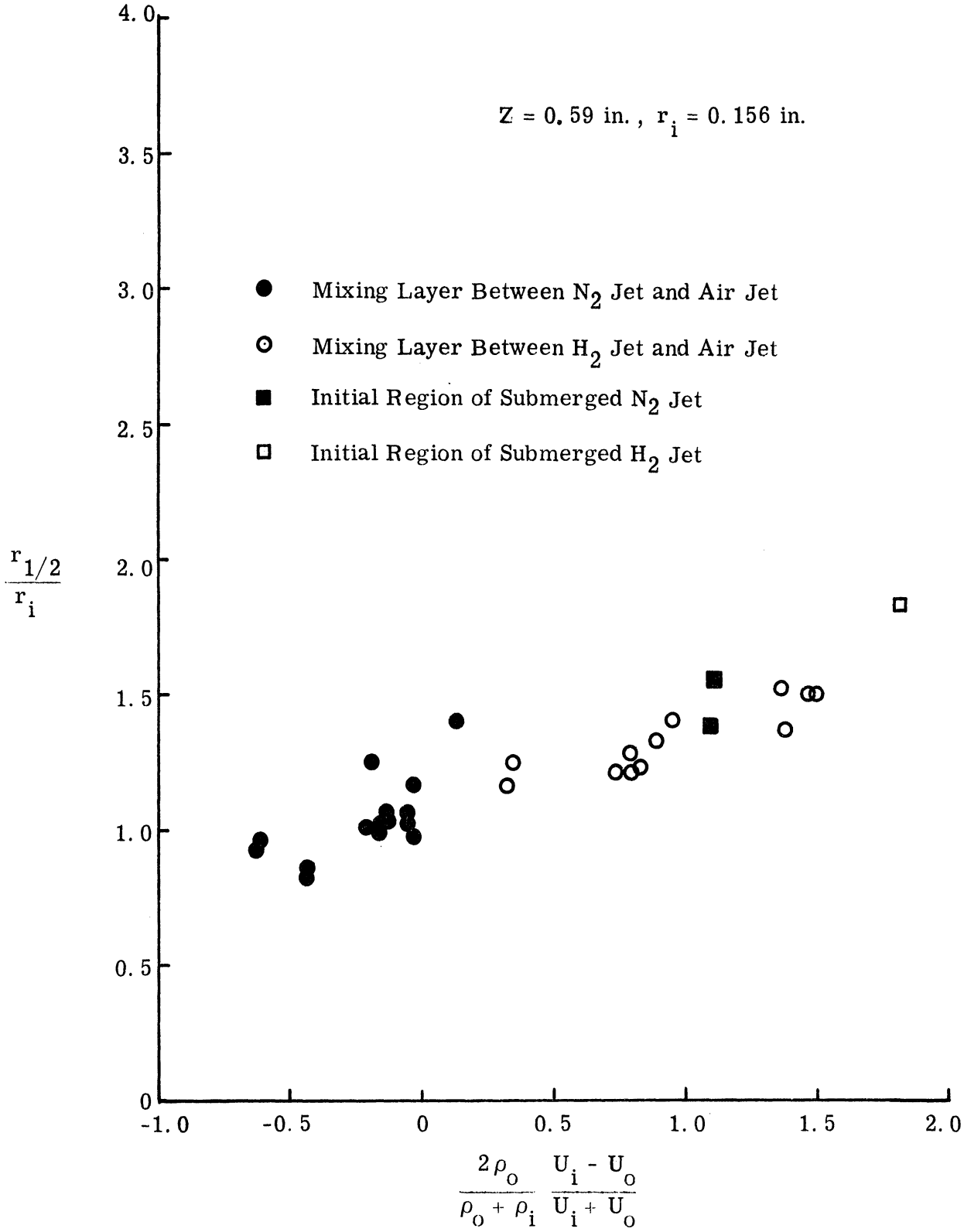

Figure 23. Half Radius Based on Partial Pressure for N_2 and H_2 Jets Mixing with Coaxial Air Jets and Ambient Atmosphere.

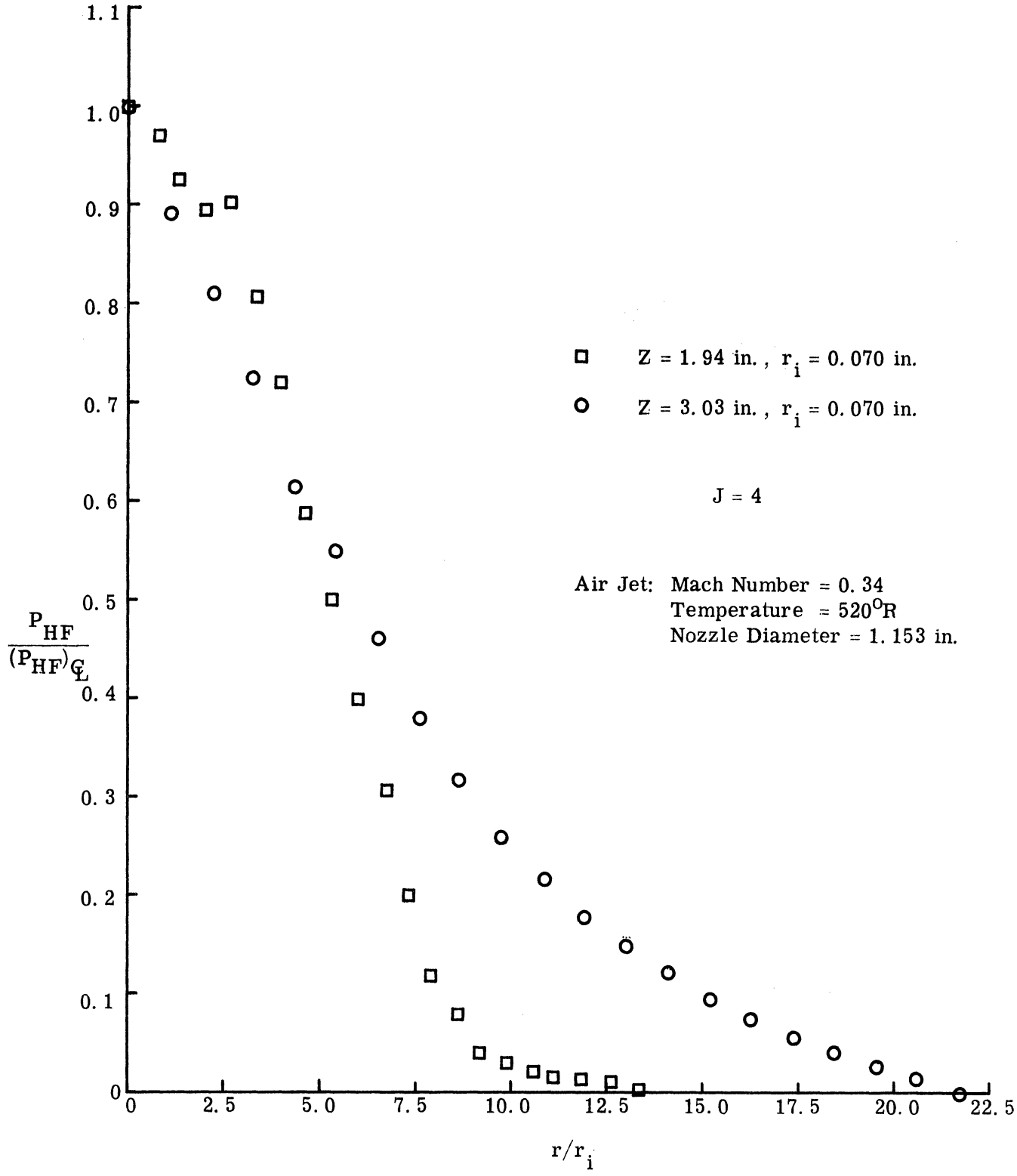

Figure 24. HF Partial Pressure Profile Resulting from Central Injection into a Subsonic Air Jet.

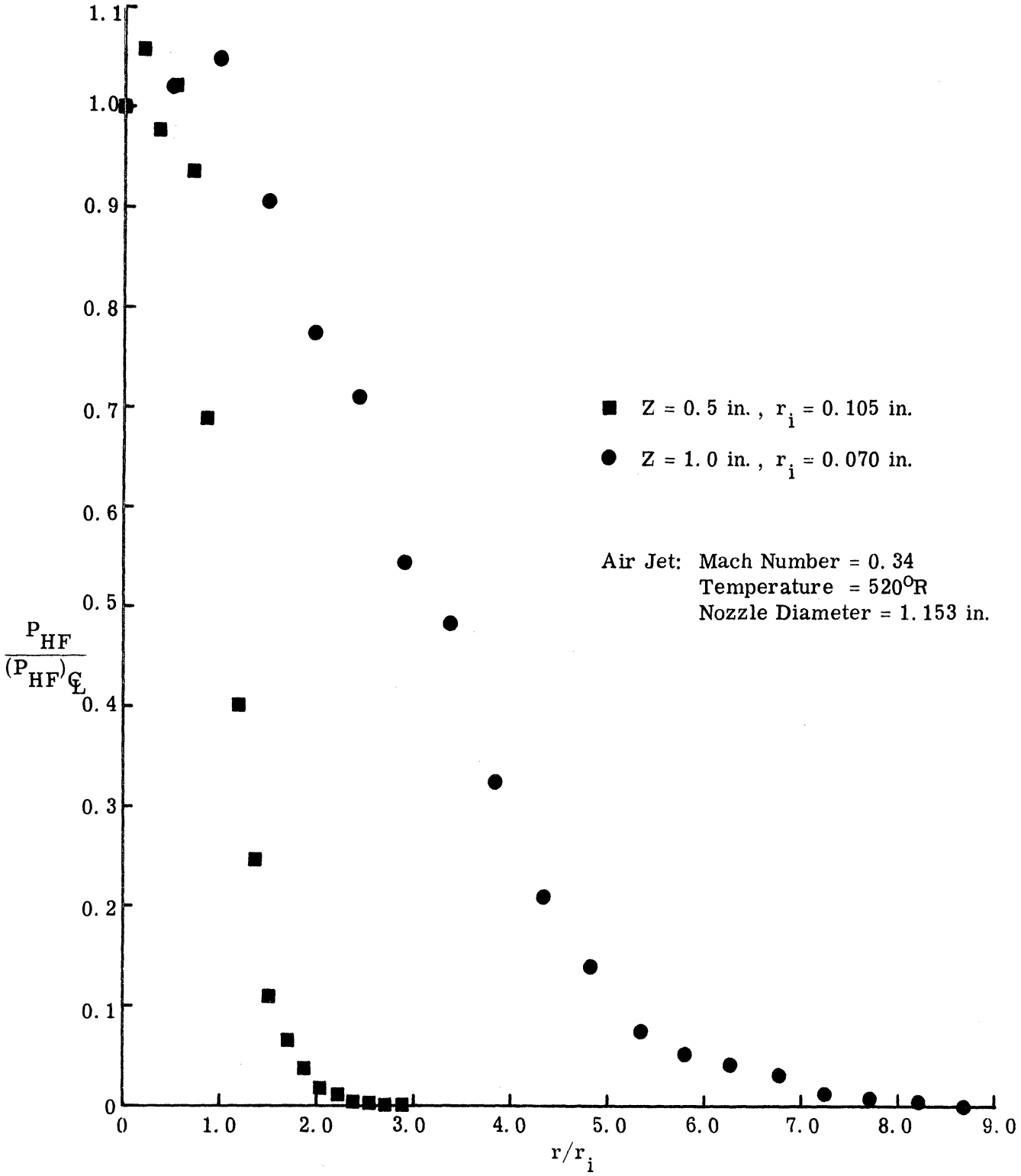

Figure 25. HF Partial Pressure Profile Resulting from Central Injection into a Subsonic Air Jet.

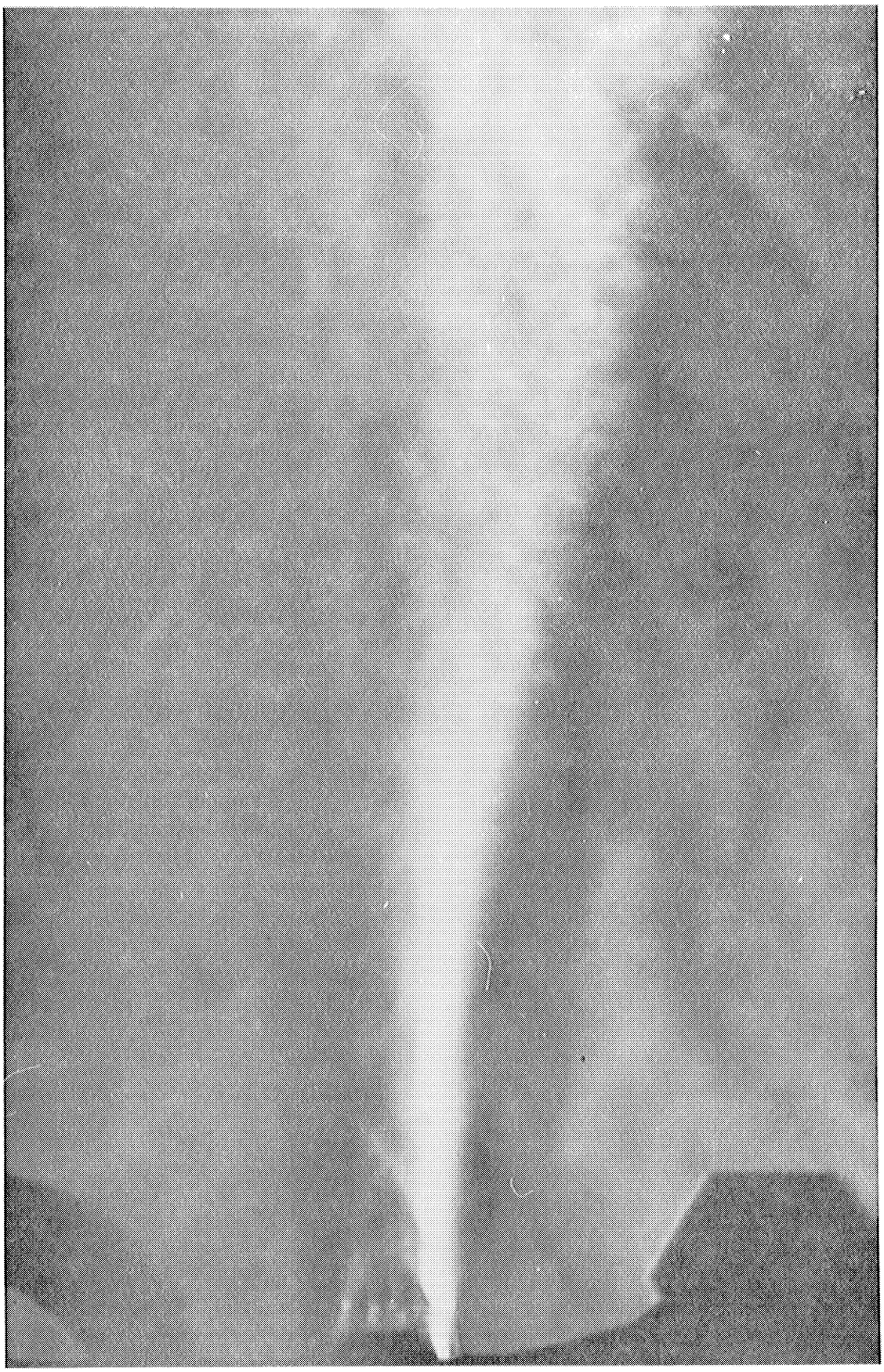

Figure 26. Vertical Knife-Edge Schlieren Photograph of Reacting H_2-Hot Air Turbulent Supersonic Jet System.

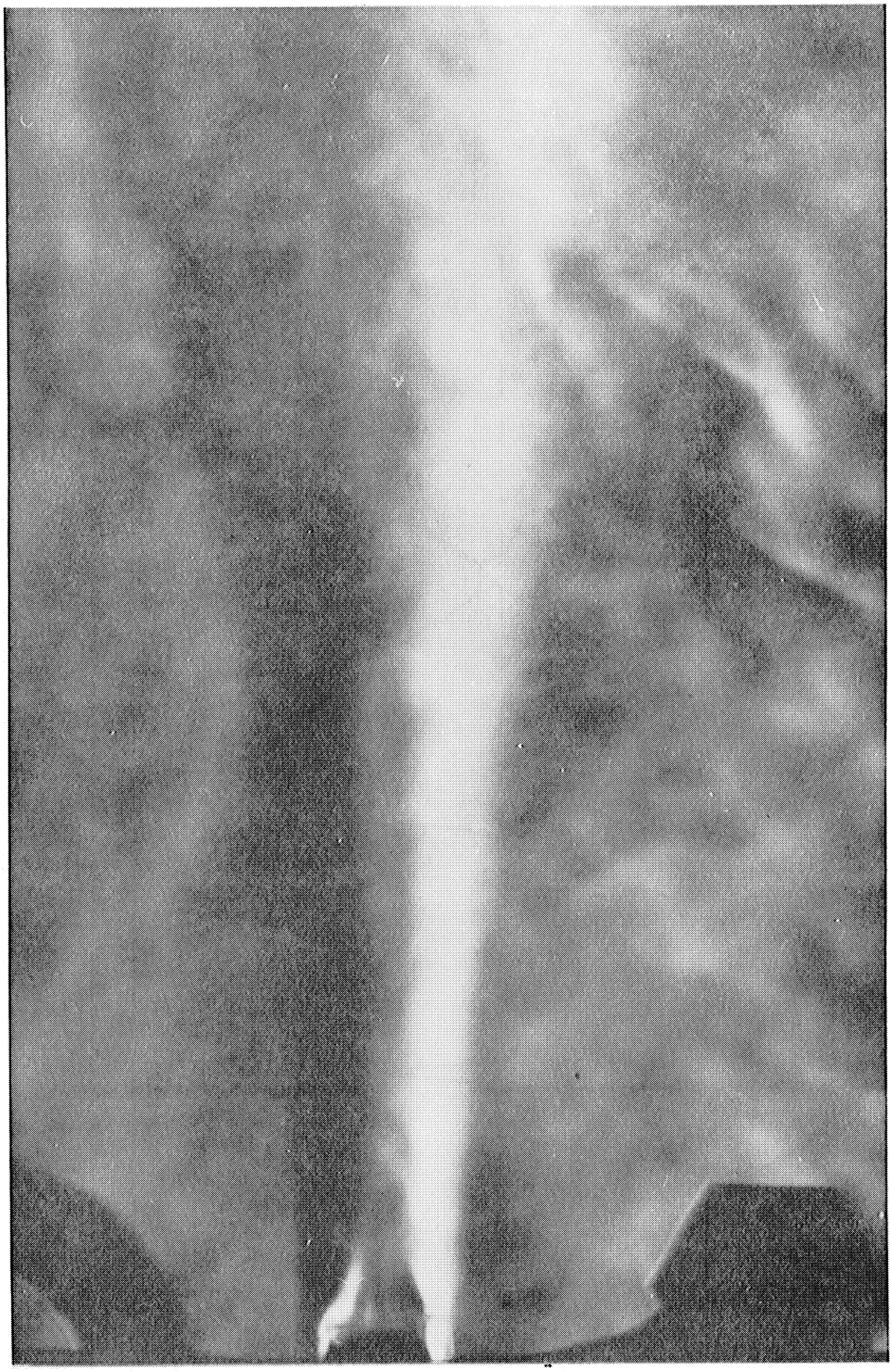

Figure 27. Vertical Knife-Edge Schlieren Photograph of Nonreacting N_2-Hot Air Turbulent Supersonic Jet System.

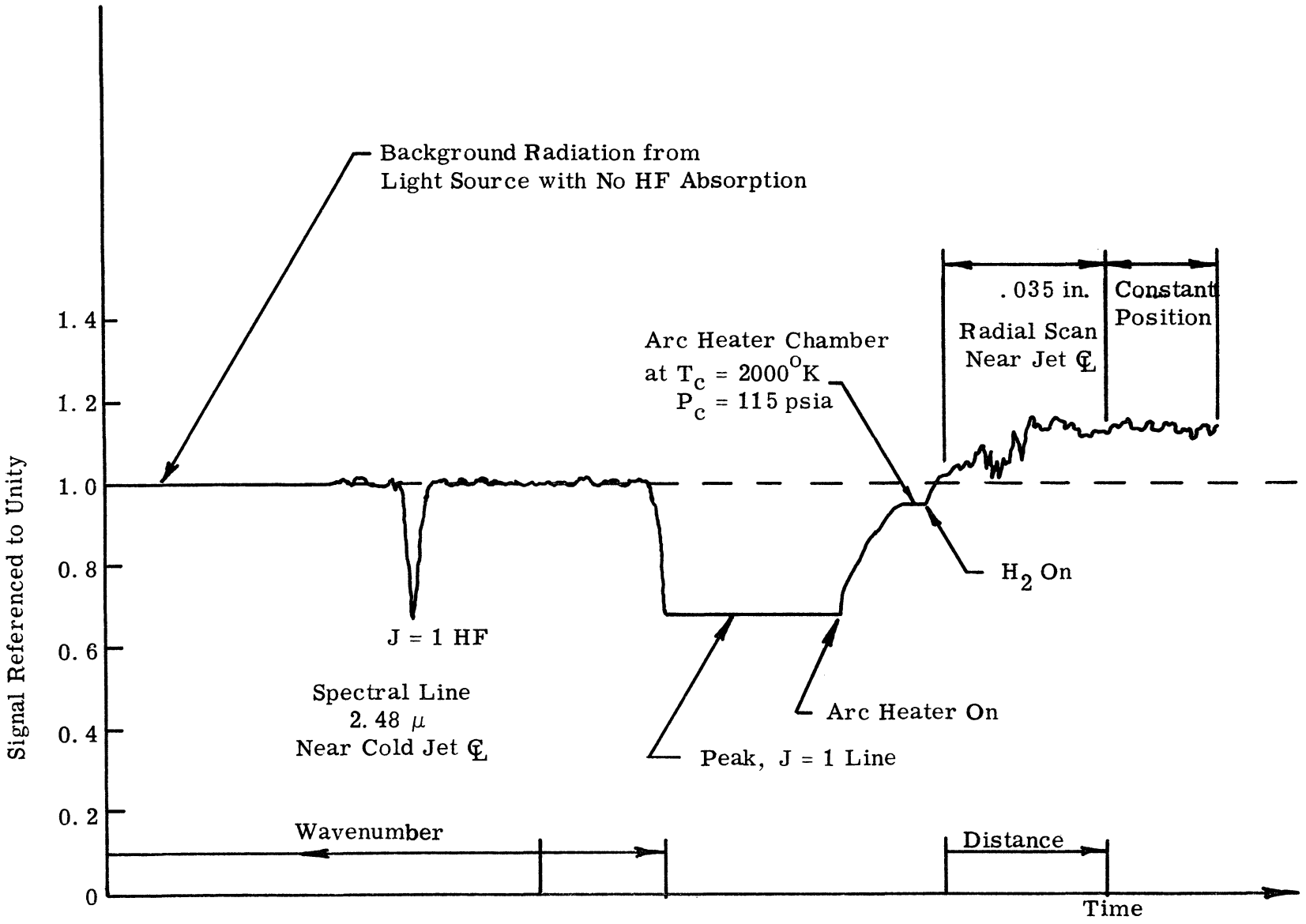

Figure 28. Spectroscopic Output during Supersonic Combustion at 2.48 microns.

REFERENCES

1. Sforza, P. M. and Trentecoste, N., "Turbulent Mixing: A Review, Reevaluation, and Extension," AIAA Paper No. 69-31, January 1969.

2. LaPointe, C. W., "Supersonic Mixng and Combustion," Air Force Aero Propulsion Laboratory Report AFAPL-TR-68-12, Wright-Patterson Air Force Base, March 1968.

3. LaPointe, C. W., "An Experimental Study of Coaxial Turbulent Mixing of Liquid and Gaseous Fuel with Air," Air Force Aero Propulsion Laboratory Report AFAPL-TR-69-64, Wright-Patterson Air Force Base, August 1969.

4. Schetz, J. A., "Analysis of the Mixing and Combustion of Gaseous and Particle-Laden Jets in an Air Stream," AIAA Paper No. 69-33, January 1969.

5. Demetriades, A., "Turbulence Measurements in an Axisymmetric Compressible Wake," Physics of Fluids, Vol. II, September 1968.

6. Laufer, J., "Turbulent Shear Flows of Variable Density," AIAA J., Vol. 7, April 1969.

7. Ting, L. and Libby, P. A., "Remarks on the Eddy Viscosity in Compressible Mixing Flows," Journal of the Aerospace Sciences, Vol. 27, October 1960.

8. Abramovich, G. N., The Theory of Turbulent Jets, M. I. T. Press, 1963.

9. Abramovich, G. N., Yakovlavsky, O. V., Smirnova, I. P., Secundov, A. N., and Krasheninnikov, S. Yu, "An Investigation of the Turbulent Jets of Different Gases in a General Stream," Astronautica Acta, Vol. 14, No. 3, 1969.

10. Glass, D. R., "The Effects of Acoustic Feedback on the Spread and Decay of Supersonic Jets," AIAA Paper, No. 68-80, January 1968.

11. Wooldridge, C. E. and Muzzy, R. J., "Boundary-Layer Turbulence Measurements with Mass Addition and Combustion," AIAA J., Vol. 4, November 1966.

12. Heyman, R. J., Sanderson, R. J., and Steel, P. C., "Combustion in Compressible Mixing Flows," Paper No. 68-20, Fall Meeting of the Combustion Institute Western States Section, Menlo Park, California, October 1968.

13. Eschenroeder, A. Q., "Intensification of Turbulence by Chemical Heat Release," Physics of Fluids, Vol. 7, November 1964.

14. Eschenroeder, A. Q. and Chen, Tung, "The Spectrum of Turbulence in an Exothermal Gas Flow," GM Defense Research Laboratories Report TR 63-217F, November 1963.

15. Malte, P. C., "Turbulent Transport in a Combusting Shear Flow," Paper No. 68-27, Fall Meeting of the Combustion Institute, Western States Section, Menlo Park, California, October 1968.

16. Hinze, J. O., Turbulence, McGraw-Hill Book Company, Inc., 1969.

17. Liepmann, H. W. and Roshko, A., Elements of Gasdynamics, John Wiley and Sons, Inc., 1957.

18. Cohen, L. S., "An Analytical Study of the Mixing and Non-Equilibrium Chemical Reaction of Coflowing Compressible Streams," AIAA Paper, No. 66-617, June 1966.

19. Geister, D. E., "Characteristics of a High Pressure AC Arc Heater System," Aerospace Research Laboratories Report, No. 67-0217, Wright-Patterson Air Force Base, December, 1967.

20. Krull, H. G. and Beale, W. T., "Effect of Plug Design on Performance Characteristics of Convergent Plug Exhaust Nozzles," NACA Report R M E 54 H05, October 1954.

21. Krull, H. G. and Beale, W. T., "Effect of Outer-Shell Design on Performance Characteristics of Convergent-Plug Exhaust Nozzles," NACA Report, E 54 K22, April 1955.

22. Winovich, W., "On the Equilibrium Sonic-Flow Method for Evaluating Electric-Arc Air-Heater Performance," NASA Report TN D-2132, 1964.

23. Shapiro, A. H., The Dynamics and Thermodynamics of Compressible Fluid Flow, Vol. I, The Ronald Press Co., 1953.

24. Simmons, F. S., "Infrared Spectroscopic Study of Hydrogen Fluoride Flames," Ph. D. Thesis, The University of Michigan, 1966.

25. Simmons, F. S., "Spectroscopic Pyrometry of Gases, Flames, and Plasmas," ISA Transactions, Vol. 2, No. 2, 1963.

26. Matheson Gas Data Book, Fourth Edition, The Matheson Gas Co., Inc., 1966.

27. Simons, J. H., Fluorine Chemistry, Vol. I, Academic Press Inc., 1950.

Unclassified

Security Classification

DOCUMENT CONTROL DATA - R & D

(Security classification of title, body of abstract and indexing annotation must be entered when the overall report is classified)

1. ORIGINATING ACTIVITY *(Corporate author)*
The University of Michigan

2a. REPORT SECURITY CLASSIFICATION
Unclassified

2b. GROUP

3. REPORT TITLE
Hydrogen Fluoride Tracer Molecule Spectroscopy Applied to Turbulent Mixing and Combustion

4. DESCRIPTIVE NOTES *(Type of report and inclusive dates)*
Technical Report

5. AUTHOR(S) *(First name, middle initial, last name)*
Philip C. Malte
James A. Nicholls

6. REPORT DATE	7a. TOTAL NO. OF PAGES	7b. NO. OF REFS
May 1970	81	27

8a. CONTRACT OR GRANT NO.	9a. ORIGINATOR'S REPORT NUMBER(S)
F33615-67-C-1122	
b. PROJECT NO.	
c.	9b. OTHER REPORT NO(S) *(Any other numbers that may be assigned this report)*
d.	AFAPL-TR-70-21

10. DISTRIBUTION STATEMENT
This document is subject to special export controls and each transmittal to foreign governments or foreign nationals may be made only with prior approval of the Air Force Aero Propulsion Laboratory (APRT), Wright-Patterson AFB, Ohio 45433.

11. SUPPLEMENTARY NOTES	12. SPONSORING MILITARY ACTIVITY
	Air Force Aero Propulsion Laboratory Wright-Patterson AFB, Ohio

13. ABSTRACT

Turbulent mixing between coaxial streams of dissimilar gases is experimentally studied. The inner stream is tagged with a tracer molecule, hydrogen fluoride. Species concentrations and turbulent mixing extents are determined spectroscopically. Details of the technique for radiatively absorbing cold jets are given.

Experiments with cold jets at subsonic and transonic Mach numbers show that the mixing layer width increases with nondimensional mass flux difference, and decreases with increasing Mach number level.

Supersonic mixing and combustion of hydrogen and air is obtained using a three phase AC arc heater to heat the air. Schlieren photographs show a substantial increase in the rate of jet spread when combustion occurs. Preliminary determinations of temperature and concentration profiles, using the HF tracer, are presented.

DD FORM 1 NOV 65 1473

Unclassified

Security Classification

14. KEY WORDS	LINK A		LINK B		LINK C	
	ROLE	WT	ROLE	WT	ROLE	WT
Turbulent Mixing Supersonic Combustion Spectroscopy Hydrogen Fluoride Tracer						